

Observational Tests and Predictive Stellar Evolution

P. A. Young, E. E. Mamajek, David Arnett and James Liebert

Steward Observatory, University of Arizona, 933 N. Cherry Avenue, Tucson AZ 85721

payoung@as.arizona.edu, eem@as.arizona.edu, darnett@as.arizona.edu,
jliebert@as.arizona.edu

ABSTRACT

We compare eighteen binary systems with precisely determined radii and masses from 23 to $1.1 M_{\odot}$, and stellar evolution models produced with our newly revised code TYCHO. “Overshooting” and rotational mixing were suppressed in order to establish a baseline for isolating these and other hydrodynamic effects. Acceptable coeval fits are found for sixteen pairs without optimizing for heavy element or helium abundance. The precision of these tests is limited by the accuracies of the observed effective temperatures. High dispersion spectra and detailed atmospheric modeling should give more accurate effective temperatures and heavy element abundances. PV Cas, a peculiar early A system, EK Cep B, a known post-T Tauri star, and RS Cha, a member of a young OB association, are matched by pre-main sequence models. Predicted mass loss agrees with upper limits from IUE for CW Cep A and B. Relatively poor fits are obtained for binaries having at least one component in the mass range $1.7 < M/M_{\odot} < 2.6$, whose evolution is sensitive to mixing. These discrepancies are robust and consistent with additional mixing in real stars. The predicted apsidal motion implies that massive star models are systematically less centrally condensed than the real stars. If these effects are due to overshooting, then the overshooting parameter α_{OV} increases with stellar mass. The apsidal motion constants are controlled by radiative opacity under conditions close to those directly measured in laser experiments, making this test more stringent than possible before.

Subject headings: binaries: eclipsing - stars: evolution - stars: fundamental parameters - hydrodynamics - stars: apsidal motion - atomic processes

1. INTRODUCTION

Prior to any rigorous investigation of thermonuclear yields, mixing, rotation, mass loss, and other complex phenomena in the evolution of stars, it is necessary to insure that the methodology used can reproduce observations at the current state of the art. Detached, double-lined eclipsing binaries provide the most accurate source of information on stellar masses and radii, and as such provide a crucial test for models of stellar evolution (Andersen 1991).

The predictive power of such simulations depends upon the extent to which the validity of their oversimplifications can be tested. Phenomenology is particularly pernicious in that good tests, which could give rise to falsification of the models and thus to progress, can be nullified by parameter adjustment (“calibration”). Similarly, the inclusion of new processes in the simulations is often contentious in that there may be several candidates put forward as the cause of the puzzling data. The treatment of the boundaries of convection zones (“overshooting”) is ripe for re-examination in terms of the underlying hydrodynamics (Asida & Arnett 2000). To aid this development, we wish to understand just how well a standard convective treatment can do (i.e., we turn overshooting off). A more physically sound procedure will be presented subsequently. Parameterized overshooting has been widely discussed (see Maeder (1975) for an early discussion, and Schröder et al. (1997) and Schaller et al. (1992); Bressan et al. (1993); Dominguez et al. (1999) for a recent ones with extensive references). Rotation also may cause mixing (Meynet & Maeder 2000). Within the context of a plasma, rotation and convection may generate magnetic fields, which by their buoyancy and angular momentum transport may provide additional causes for mixing.

This paper represents a first step toward testing our extensively revised stellar evolution and hydrodynamics code, TYCHO. Our goals are (1) the understanding the predictive capability of stellar evolution theory by the critical re-evaluation of its assumptions, and of its underlying basis in observations and in laboratory data, (2) the examination of the tricky problem of mixing in stars to help design experiments (Remington et al. 1999) and numerical tests (Asida & Arnett 2000), and (3) the development of an open source, publicly available stellar evolution code with modern capabilities for community use.

1.1. Choice of Binaries

The most comprehensive list of binary systems with accurately measured masses and radii is given in the review by Andersen (1991). A subset of the original binaries was chosen for this exploratory effort. The systems with the smallest uncertainties were picked such that the range of masses from 23 to $1.1 M_{\odot}$ was well sampled. The upper mass limit is the largest mass present in the data, while the lower limit is safely above the point at which the equation of state used in the modeling becomes inaccurate. This is primarily due to approximate treatment of Coulomb contributions to the pressure; we use only the weak screening limit for the plasma. The Coulomb interaction leads to a negative pressure correction of $\sim 8\%$ in the outer part of the convection region and $\sim 1\%$ in the core for a star of $1 M_{\odot}$ (Däppen & Nayfonov 2000), and is less important for more massive stars. We obtain a comparable correction to the central pressure for a solar model (-1.7%).

Aside from the exclusion of stars of still lower mass, no bias was applied in the selection process. For stars of $1 M_{\odot}$ or less, the issue of possible overshooting in the convective core is moot because their cores are radiative. Also, because they rotate rapidly only for a brief part of their lives, rotational mixing is expected to be less than for our selected stars. The binaries used in the

study along with their fundamental parameters are presented in Table 1. Ribas et al. (2000) have revised the Andersen (1991) temperature estimates, and revised estimates for the masses of EM Car (Stickland, Lloyd, & Corcoran 1994) and CW Cep (Stickland, Koch & Pfeiffer 1992) have been presented. Latham et al. (1996) have revised the parameters for DM Vir. All these changes are incorporated into Table 1.

1.2. The Mixing Length

If the purpose of a stellar evolution code is to make testable predictions of the behavior of stars, then the adjustment of the mixing length by fitting stellar data is repugnant. Alternatives are to constrain it by experiment or by simulation. At present we know of no definitive experimental results which determine the mixing length appropriate to stars, although a variety of experiments do test other aspects of stellar hydrodynamics and the codes used to simulate them (Remington et al. 1999). However, it is becoming possible to simulate turbulent, compressible convection with sufficient realism to constrain the range allowed for the mixing length (Rosenthal et al. 1999; Porter & Woodward 1994, 2000; Elliott, Miesch, & Toomre 2000; Asida 1998). Porter & Woodward (2000) find a mixing length $\alpha_{ML} = 2.68$ in units of pressure scale height; this is based upon simulations having mesh resolutions as high as $512 \times 512 \times 256$ and corresponding Rayleigh numbers as high as 3.3×10^{12} . Rosenthal et al. (1999) based their work on resolutions up to $253 \times 253 \times 163$, but with a more realistic treatment of radiative transfer and ionization. They were able to synthesize the line profile of FeII $\lambda 5414$ which compared well with that observed. Their results agreed with standard 1-D models, although they suggest that this might be “the right result for the wrong reason.” Standard models use $\alpha_{ML} = 1.5$ to 2, which is significantly smaller than the value of Porter & Woodward (2000). For a red giant, Asida (1998) inferred $\alpha_{ML} = 1.6$, based upon 2-D simulations but with fairly realistic microphysics.

Canuto & Mazzitelli (1991, 1992) have proposed a serious model to replace mixing length theory; this has had the salutary effect of shifting the debate to the physics of convection and away from the best choice of mixing length. Finally, Asida & Arnett (2000) have shown from 2-D simulations that the underlying physical picture for stellar convection is incomplete, even in the deep interior where the complication of radiative transfer is minor.

We simply choose $\alpha_{ML} = 1.6$, and look forward to the convergence of these efforts to provide a convection algorithm which is independent of stellar evolutionary calibrations.

1.3. The TYCHO Code

The evolutionary sequences were produced with the TYCHO stellar evolution code. The code was originally developed for one dimensional (1D) hydrodynamics of the late stages of stellar evolution and core collapse (Arnett 1996). It is being completely rewritten as a general purpose, open

source code for stellar evolution and hydrodynamics. The present version is written in structured FORTRAN77 and is targeted for Linux machines. It has been successfully ported to SunOS and SGI IRIX operating systems. It has extensive online graphics using PGPLOT, an open source package written by T. J. Pearson (tjp@astro.caltech.edu). A library of analysis programs is being built (modules for apsidal motion, pulsational instability, reaction network links, and history of mass loss are now available). The code is being put under source code control to allow versioning (this will allow particular versions of the code—for example the one used in this paper, to be resurrected accurately at later times), and to improve the reproducibility of results.

Knowledge of the radiative opacity of plasma at stellar conditions has changed qualitatively in the past decade. Historically, solar and stellar atmospheres provided much of the empirical data on hot plasmas. For example, Kurucz (1991) tabulates a range of effective temperatures from 2,000 to 200,000 K. These temperatures and the corresponding (low) densities characterized what was directly observable. Higher temperatures could be found at lower densities (in non-LTE) or indirectly inferred by use of theoretical models. Terrestrial tests involved explosions which were difficult to quantify with adequate precision to determine opacity. Measurements of opacity in a well characterized, hot, dense, laser-produced plasma have become possible (Perry et al. 1991; Springer et al. 1992; Mostovych et al. 1995; Davidson et al. 2000). The first experiments to simultaneously quantify temperature and density with good precision (Perry et al. 1991; Springer et al. 1992) involved temperatures $T \approx 7 \times 10^5$ K and densities $\rho \approx 2 \times 10^{-2}$ g cm $^{-3}$, which are directly relevant to stellar evolution and to apsidal motion. The range of conditions which are experimentally accessible is expanding with the development of new instruments and techniques. Not only can direct measurements be made, but complex and sophisticated theories of the physical state of the plasma can be tested, giving more reliable extrapolations into conditions not yet experimentally accessible (Perry et al. 1996; Davidson et al. 2000). The conditions just quoted are encountered in stars of about $1M_{\odot}$, and are important for stellar evolution (see Ch. 7, Arnett (1996)).

The opacities used here are from Iglesias & Rogers (1996) and Kurucz (1991), for a solar abundance pattern (Anders & Grevesse 1989). The Iglesias & Rogers (1996) opacities were computed with 21 elemental species; Iglesias et al. (1995) have shown that the remaining elements are so rare as to have only a marginal effect on the Rosseland mean opacities (for solar relative abundances of the heavier elements). While the OPAL opacities were constructed for astrophysical use, the underlying experiments and theoretical models are determined by the inertial confinement fusion (ICF) community, reducing the danger of unconscious bias from astronomical puzzles leaking back into the construction of opacities. Extension of the opacity library to lower temperatures and lower entropies is planned.

TYCHO is designed to use an adaptable set of reaction networks; for these calculations, two networks were used. At higher temperatures ($T \geq 10^7$ K), an 80 element reaction network was solved. The reaction rates were from F. K. Thielemann (private communication); see also (Thielemann, Arnould, & Truran 1988). For lower temperatures this was replaced by a 15 element network which was designed for deuterium, lithium, beryllium, and boron depletion. The reaction rates were

from Caughlan & Fowler (1988). The match at the temperature boundary was sufficiently good as to require no smoothing. More recent compilations of nuclear rates are available (Rauscher & Thielemann 2000; Angulo et al. 1999), but were not used here to simplify the comparison with previous work.

The outer boundary condition was determined by use of the Eddington approximation to a grey, plane parallel atmosphere, integrated in hydrostatic equilibrium inward to a fitting point for the interior. For the most extended model considered here, the ratio of mean free path to radius was $\lambda/R \sim 5 \times 10^{-3}$, so that spherical effects are negligible. The most vigorous mass loss considered was so mild that the ram pressure ρv_{loss}^2 at the photosphere was 10^{-6} of the total thermal pressure, which is consistent with the hydrostatic assumption. Such integrations were used to define the pressure and temperature at the fitting points, $T_f(L, R)$ and $P_f(L, R)$, for the stellar luminosity L and radius R . Their derivatives with respect to stellar luminosity and radius were approximated by finite differences constructed between three such integrations (at L, R , $L + \delta L$, and $L, R + \delta R$). Typically, of order 200 to 400 steps were used in the envelope integration.

We used Schwarzschild convection as formulated by Kippenhahn & Wiegert (1990), and our treatment of convective overshooting was turned off.

Mass loss was included and based on the theory of Kudritzki et al. (1989) for $T_{eff} \geq 7.5 \times 10^3$ K and the empirical approach of de Jager, Nieuwenhuijzen, & van der Hucht (1988) for lower effective temperatures. R. Kudritzki kindly provided appropriate subroutines for the hotter regime. Even for EM Car, the most massive system in the list, the effects of mass loss were modest (0.6 to $0.7 M_\odot$).

The equation of state was that discussed in Timmes & Arnett (1999), augmented by the solution of the ionization equilibrium equations for H, He, and a set of heavier elements scaled from the solar abundance pattern. Both the equation of state and the thermonuclear reaction rates are affected by coulomb properties of the plasma. Only weak screening was necessary here. Extension to include both weak and strong screening consistently in the equation of state and thermonuclear reaction rates is planned; previous versions of the code included strong screening as well.

Models were run for each mass, starting with a fully convective initial model on the Hayashi track and ending well beyond hydrogen depletion in the core. A more realistic approach would have been to form the stars by accretion (A. G. W. Cameron, private communication; Norberg & Maeder (2000)). We justify our choice by its simplicity, and by noting that only the last stages of the pre-main sequence are relevant here, for which the two cases give similar results.

Zoning in the interior typically ranged from 200 to 500 zones. All runs had solar heavy element abundance (Anders & Grevesse 1989) and used a ratio of mixing length to scale height of $\alpha = 1.6$ for convection. This choice gave a reasonably good solar model when compared to Bahcall & Pinsonneault (1998) and Christensen-Dalsgaard (2000); inclusion of element settling by diffusion and adjustment of the helium abundance would give improved consistency for the present-day sun, but diffusion would have less time to operate in the more massive stars considered here. Rotational mixing was turned off.

1.4. Related Investigations

The stars are all at or near the main sequence, so that the possible list of citations is enormous; the efforts of the Padua group (Bressan et al. 1993), the Geneva group (Schaller et al. 1992), and the FRANEC group (Dominguez et al. 1999) have comparable input physics and form a useful context. We focus discussion on Pols et al. (1997b) and Ribas et al. (2000), who consider many of the same binaries, and Claret & Giménez (1993) who examined the apsidal motion test.

The largest differences in microphysics between Pols et al. (1997b) and this paper are our use of Iglesias & Rogers (1996) rather than Rogers & Iglesias (1992) opacities, a more realistic nuclear network, and a different approach to the equation of state, but none of this seems to be particularly significant for the issues here. We do include mass loss, but these effects are not large. Pols et al. (1997b) do not calculate the pre-main sequence evolution (which is relevant to several of our binaries). They define an overshooting parameter which is fixed by previous work on ζ Aurigae binaries (Schröder et al. 1997). They construct a grid of models in mass (0.5 to 40 M_{\odot}) and heavy element abundance ($Z = 0.01, 0.02$ and 0.03), assuming $X = 0.76 - 3.0Z$ and $Y = 0.24 + 2.0Z$ for the abundances of hydrogen and helium. They minimize a χ^2 error estimator in four parameters: the masses M_A and M_B , the age t of the binary, and Z , the heavy element abundance.

As a test of consistency for later evolution, we have reproduced the 4 and 8 M_{\odot} sequences of Pols et al. (1997a), which did not use overshooting. The notoriously sensitive blue loops were reproduced to graphical accuracy (their Figure 4) for the same input physics. The codes seem highly consistent.

Ribas et al. (2000) used the models of Claret (1995, 1997b) and Claret & Giménez (1995, 1998), which use Rogers & Iglesias (1992) opacities and a 14 isotope network and include overshooting and mass loss. They too interpolated in a grid, minimizing a χ^2 error estimator. This procedure was more complex than that used by Pols et al. (1997b), and need not be described here. Both heavy element abundance and helium abundance were freely varied.

Our strategy differs from both Pols et al. (1997b) and Ribas et al. (2000), which may provide a useful contrast. Here we are interested in isolating the possible inadequacy of the standard formulation of stellar evolution, so we avoid optimization of parameters as much as possible. By using (1) solar abundances and (2) the measured masses, we reduce the degrees of freedom, and hopefully make the possible flaws in our stellar evolution prescriptions easier to see. By the same token, our models should fit the data less well because we have not optimized abundances or masses. Mathematically, optimization will almost always improve the fit, but not necessarily for the correct reasons. However, the actual abundances may be different from our assumptions, and the masses do have error bars.

Claret & Giménez (1993) used Rogers & Iglesias (1992) opacities, solar abundances, a mixing length ratio $\alpha_{ML} = 1.5$, and overshooting of $\alpha_{OV} = 0.2$ pressure scale heights (that is, essentially the same physics as the models used by Ribas et al. (2000)), and computed structure constants for

apsidal motion for seven of the binaries we consider (EM Car, CW Cep, QX Car, U Oph, ζ Phe, IQ Per, and PV Cas).

Detailed comparisons will appear in the discussion below.

2. FITTING MODELS TO BINARIES

The first step in comparing the binary data with the computations is the choice of the best models. This was done by examining a χ^2 quantity for each binary pair, defined by

$$\begin{aligned}\chi^2 &= ((\log L(m_A, t) - \log L_A)/\sigma_{LA})^2 \\ &+ ((\log L(m_B, t) - \log L_B)/\sigma_{LB})^2 \\ &+ ((\log R(m_A, t) - \log R_A)/\sigma_{RA})^2 \\ &+ ((\log R(m_B, t) - \log R_B)/\sigma_{RB})^2,\end{aligned}\tag{1}$$

where A and B denote the primary and the secondary star, respectively. Here L_A and R_A are the observationally determined luminosity and radius of the primary, with σ_{LA} and σ_{RA} being the observational errors in $\log L_A$ and in $\log R_A$. We convert the observational data for the radii to logarithmic form for consistency. Correspondingly, $L(m_A, t)$ and $R(m_A, t)$ are the luminosity and radius of the model. This χ^2 was evaluated by computing two evolutionary sequences, one for a star of mass m_A and one for m_B , and storing selected results from each time step. Then these files were marched through, calculating χ^2 at consistent times ($t_A = t_B$ to a fraction of a time step, which was a relative error of a few percent at worst). The smallest χ^2 value determined which pair of models was optimum for that binary. Note that if the trajectories of both A and B graze the error boxes at the same time, $\chi^2 \approx 4$. These error parameters along with the corresponding uncertainties from the observations are presented in Table 2.

Figure 1 displays the resulting χ^2 for each binary pair, in order of descending mean mass. The binaries fall into three separate groups: ten have excellent fits ($\chi^2 < 4$; EM Car, V478 Cyg, CW Cep, CV Vel, U Oph, PV Cas, RS Cha, PV Pup, DM Vir and UX Men), six are marginal ($16 \leq \chi^2 \leq 4$; QX Car, ζ Phe, IQ Per, MY Cyg, EK Cep, and V1143 Cyg), and two are poor fits ($\chi^2 > 16$, denoted *offscale* in Figure 1; VV Pyx and AI Hya). The boundaries between these groups are indicated by vertical lines.

2.1. Global Aspects of the Errors

The weakness of a χ^2 measure is that it is most meaningful if the errors have a gaussian distribution around the mean (Press et al., (1992), chapters 14 and 15), which does not seem to be the case here. In particular, systematic shifts in the empirical data, due to new analyses, can give significant shifts in the error estimation. Ribas et al. (2000) have re-estimated the effective

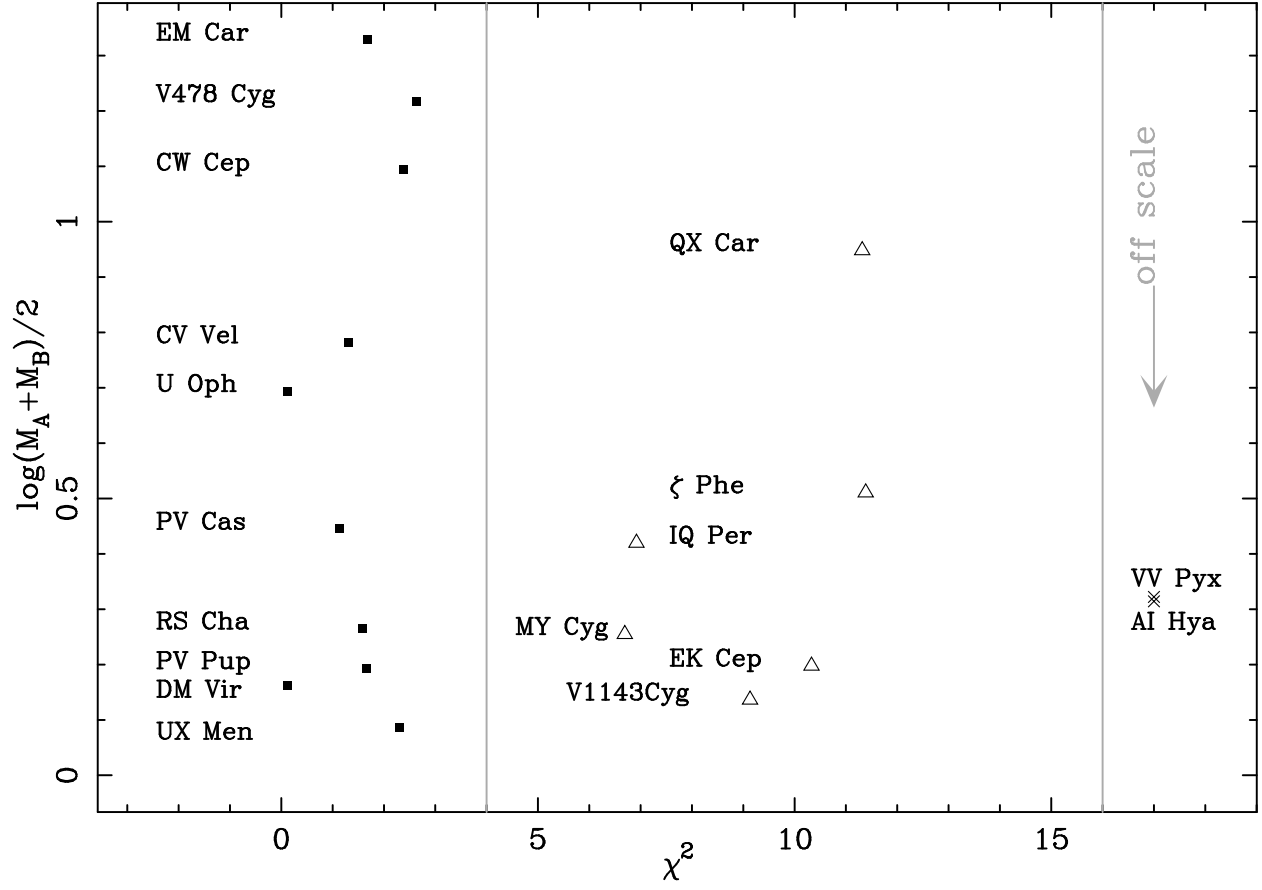


Fig. 1.— χ^2 for optimum models of selected binaries, versus mean mass of the binary.

temperatures of 13 of the 18 binaries we have examined. Five (QX Car, U Oph, PV Cas, AI Hya, and RS Cha) were changed by more than twice the error estimates of either Ribas et al. (2000) or Andersen (1991). Further, Stickland, Koch & Pfeiffer (1992) and Stickland, Lloyd, & Corcoran (1994) have analyzed additional data (from IUE) and find masses of CW Cep and EM Car which lie beyond twice the error estimates. This is to be expected if the errors are dominated by systematic effects, and warns us to distrust all but our most robust inferences.

Because the fractional errors in mass and in radius are much more restrictive, it strongly supports the need for renewed efforts to pin down the effective temperatures of these stars. The choice of L and R rather than L and T_{eff} in our definition of χ^2 is significant: the smaller errors for R make the χ^2 more discriminating. Pols et al. (1997b) use R and T_{eff} which has the slight advantage here of involving less propagation of observational errors, but because R is much more precise than T_{eff} , the effect is small for the present data.

We have chosen to update the original data of Andersen (1991), incorporating the changes made by the Ribas et al. (2000) effective temperatures and the Stickland, Koch & Pfeiffer (1992) and Stickland, Lloyd, & Corcoran (1994) masses. We have used the new data for DM Vir (Latham et al. 1996). Our general conclusions are unaffected by which of these sets of data we use.

The comparison of observed and computed stars may be presented as an goodness of fit vector, which has the advantage of being directly representable in the HR diagram for the stars. The observed points with error bars are plotted along with an arrow indicating the distance and direction to the best model point. The way in which the models differ from the observations can then be taken in at a glance. Figure 2 shows the goodness of fit vectors, from the observed points (shown with error bars) to the best model star (chosen as described above). The largest discrepancy is the secondary of VV Pyx. Of the eight binaries (QX Car, ζ Phe, IQ Per, VV Pyx, AI Hya, EK Cep, MY Cyg, V1143) which have mediocre or poor fits, seven (QX Car is the exception) have at least one component lying in the range $1.7 < M/M_{\odot} < 2.6$. Andersen, Nordström, & Clausen (1990) noticed similar behavior.

Figure 3 shows the luminosity differences between the models and the stars. The vertical axis is mass in solar units; binary components are connected by a line. The two binaries with $\chi^2 > 16$ (VV Pyx and AI Hya) are denoted by crosses; they are poor fits and should be given little weight. Considering the best fits, $\chi^2 < 4$ (solid squares), there is a dramatic trend: the highest mass models (for example, EM Car) are underluminous relative to the actual binaries, while the lower mass models are not.

Given the indications that the errors may be dominated by systematic effects, we approach a statistical discussion with caution. The two binaries which have $\chi^2 > 16$ are eliminated from this statistical discussion on the basis that these fits are too poor to be meaningful. In principle, the mean errors could show a systematic shift in the models relative to the data, but because we choose an optimum pair of models, the choice masks any absolute shift. The error should reappear as a larger RMS difference. For luminosity, the first moment of the difference between model and

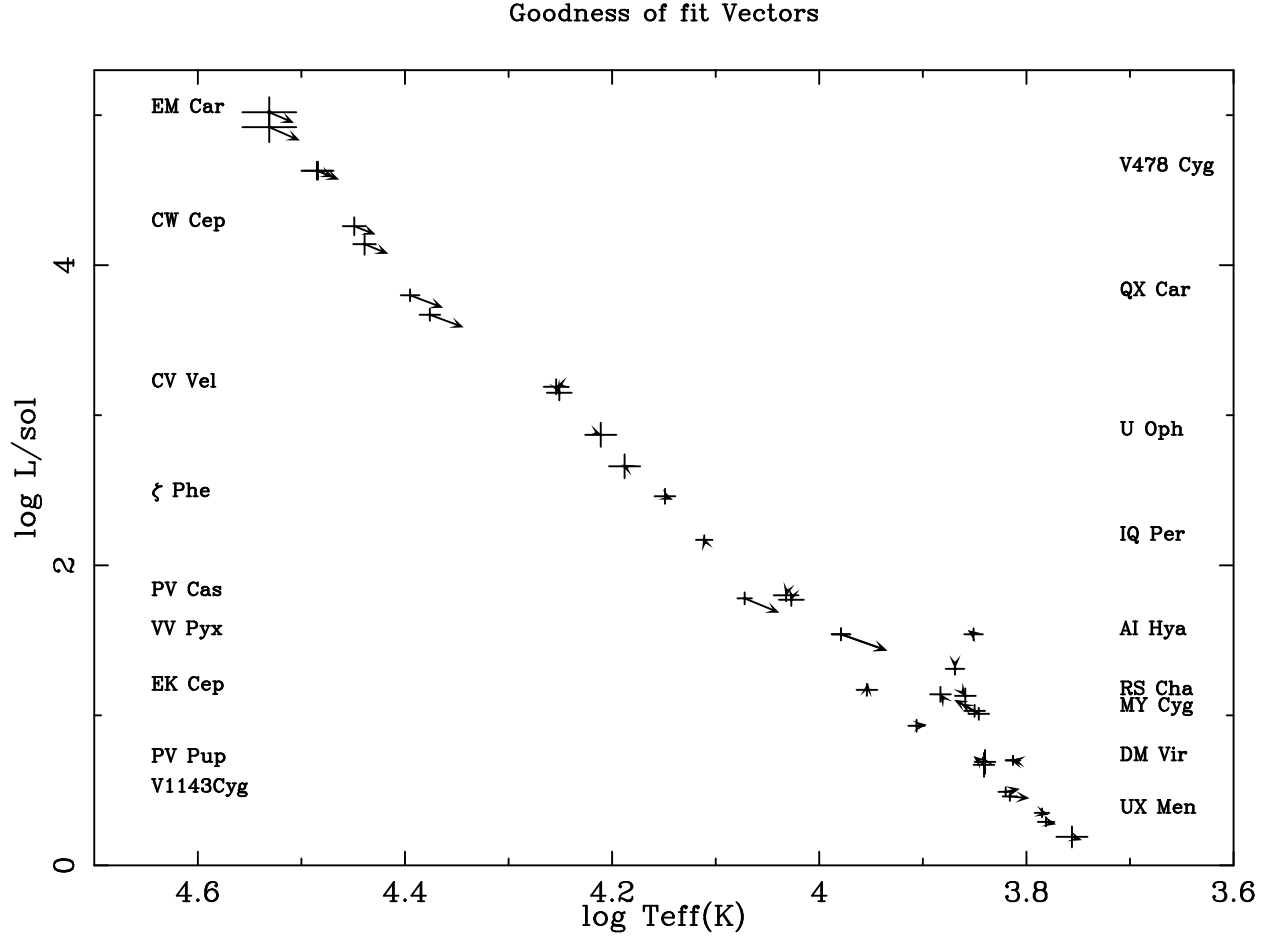


Fig. 2.— Goodness of fit vectors for selected binaries, with observational error bars.

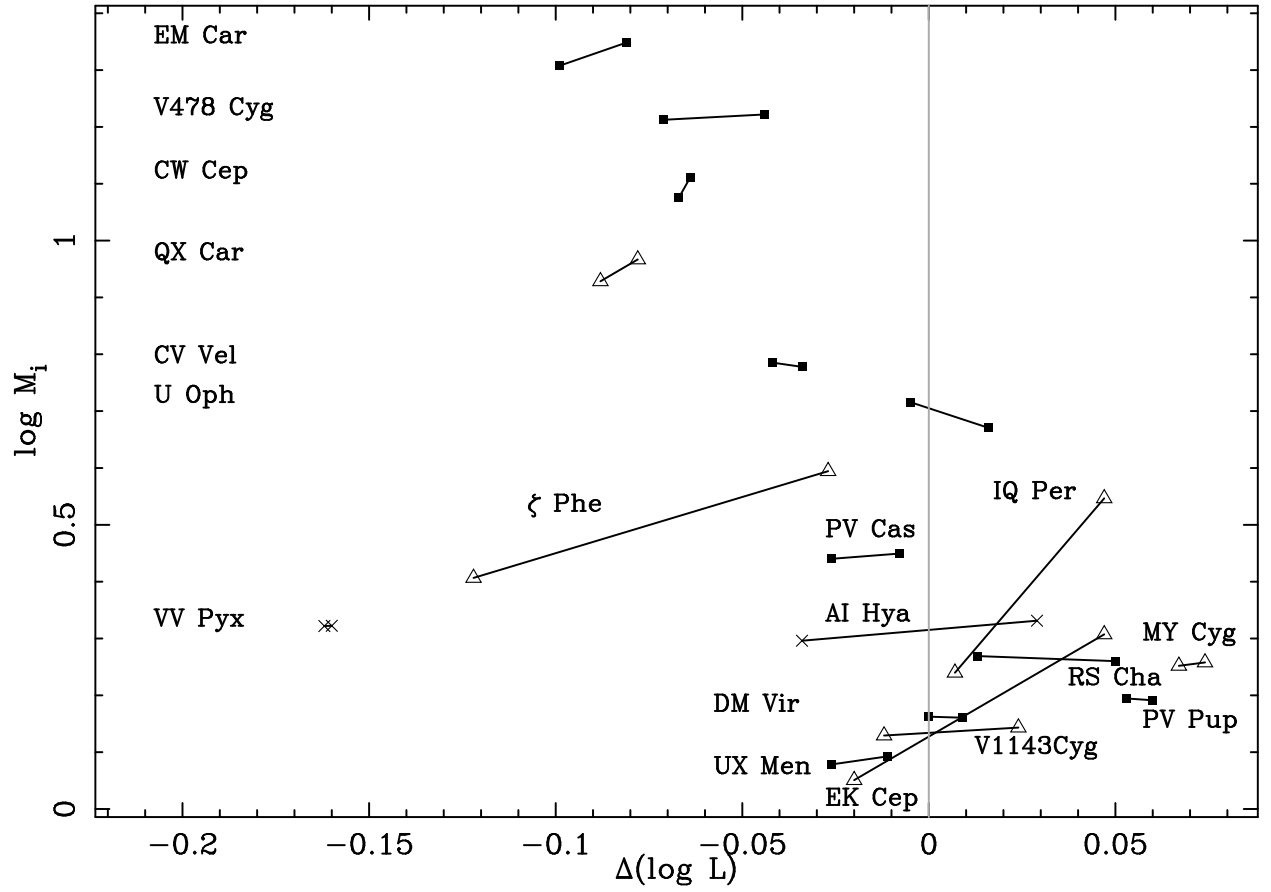


Fig. 3.— Luminosity differences between best fit models and observations.

stellar logarithmic luminosity is just the mean of this difference, which is -0.017 in the base ten logarithm (the models are too dim by this amount). The shift is smaller than the RMS error of the observational data, which is 0.056 . If there were a bad global mismatch, the RMS difference in “model minus star” would be much larger than the average error in the observations. However, the RMS difference between the models and stars is 0.054 , which is almost the same as the observational error. The luminosity is basically a measure of the leakage time for radiation, which is dominated by the value of the opacity in the radiative regions. It samples the whole star, including the deep interior. In a global sense, our mean leakage rate seems correct to the level of the statistical and observational error.

The shifts in radius between the models and the stars are shown in Figure 4. The vertical axis and the symbols are the same as in the previous figure. The mean shift is 0.0053 in the logarithm (the models are too large by this small amount); the corresponding standard error of the Andersen data for which the fits are acceptable is 0.016 , to be compared with an RMS difference between models and stars of 0.014 . Except for a few outlying cases, the distribution is fairly uniformly distributed around zero. If only the best fits (squares) are considered, a subtle trend might be inferred: 9 of 12 of the models above $4M_{\odot}$ have radii which are too large.

The corresponding mean shift in $\log T_{eff}$ is -0.007 (the models are too cool by this amount). Again, this is small in comparison to the standard error of the observations (0.014). The corresponding RMS difference between models and stars is 0.017 . The effective temperature is a surface quantity, and is more sensitive to the outer layers which contain little of the stellar mass.

These numbers suggest that standard stellar evolutionary sequences of these stages should be able to produce luminosities, radii, and effective temperatures within 11, 3 and 4 percent, respectively, of good observational data. Otherwise, new physics is indicated. Because the standard stellar evolutionary models do this well, small “improvements” may contain no information. We will emphasize systematic trends, and those implications which emerge from several independent tests.

2.2. Massive Binaries

Figure 5 shows the evolution of the model stars in log luminosity and log radius, for EM Car, V478 Cyg, CW Cep, QX Car, CV Vel, and U Oph, corresponding to a mass range from 23 to $4.6 M_{\odot}$. Except for QX Car ($\chi^2 = 11.3$), models of these binaries have $\chi^2 < 4$, and so represent good fits. The error bars are centered on the observed stars; the arrows point from them to the optimum models. Notice the the fits can be multivalued because the trajectories may pass through the error boxes multiple times. This is shown occurring first as the model descends from the pre-main sequence (pre-MS), and again during main sequence hydrogen burning. If the stellar masses are significantly different, this ambiguity is removed by the condition that both components have the same age. All the model stars are too dim (all the arrows point downward), a signal that the

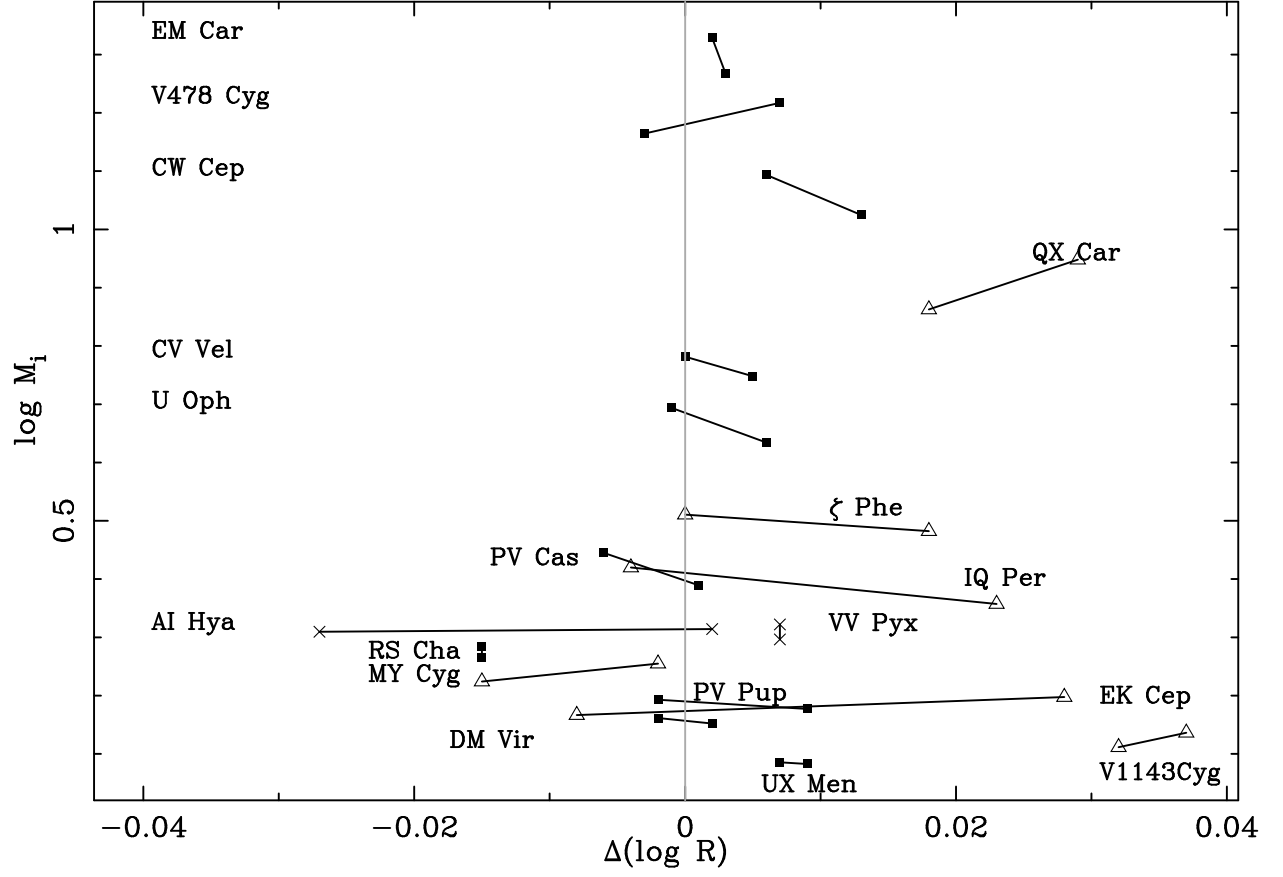


Fig. 4.— Radius differences between best fit models and observations.

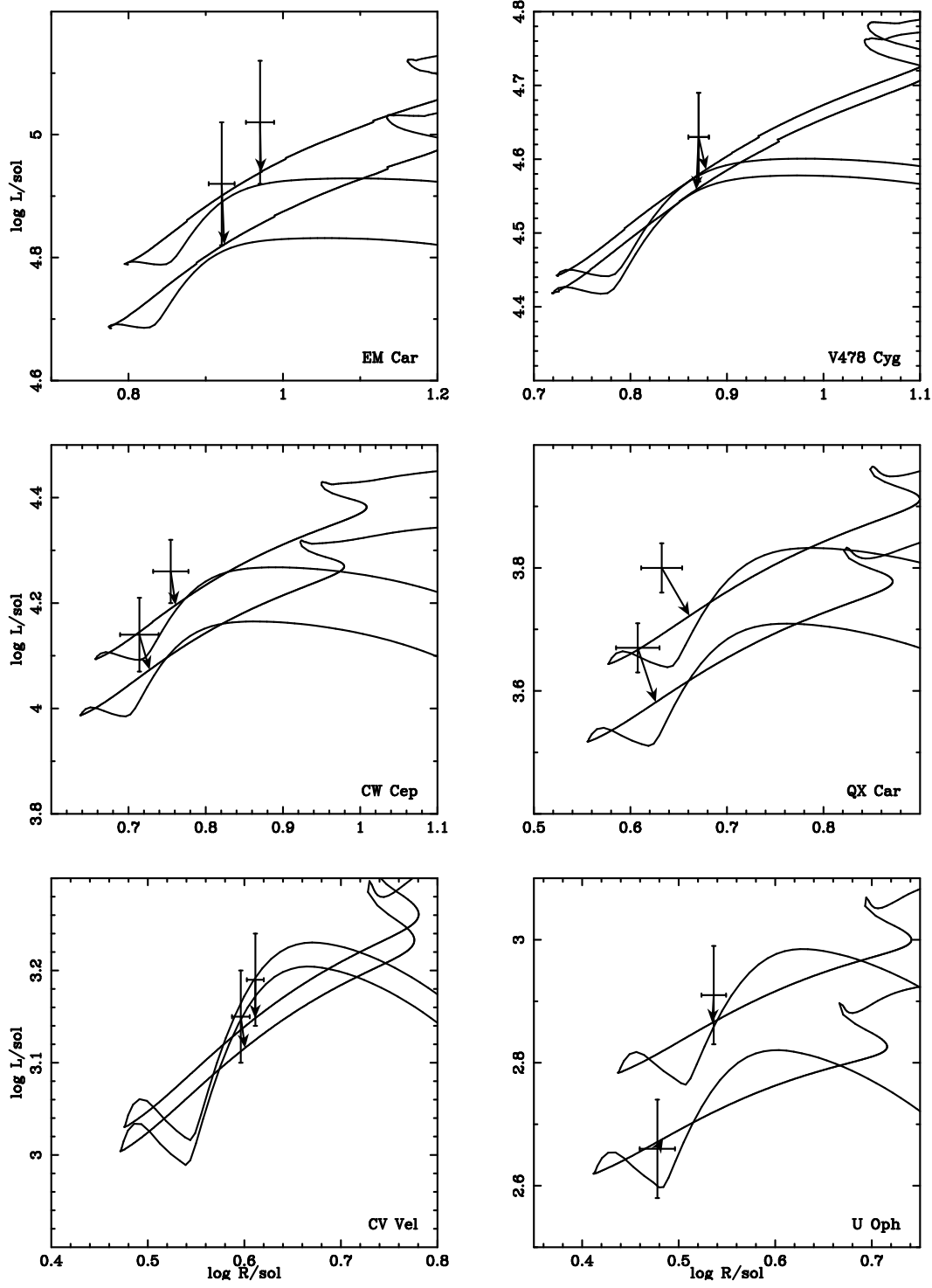


Fig. 5.— Massive models: EM Car, V478 Cyg, CW Cep, QX Car, CV Vel and U Oph. The masses range from 23 to $4.6 M_{\odot}$.

standard stellar evolution prescription is systematically wrong.

EM Car, being the most massive system, also has the most significant mass loss. The model evolutionary sequences are set by the choice of initial mass, but the observational constraint on mass is applied after the best fitting model is determined. This is an implicit function of the choice of initial mass, and iteration is required. Initial masses of 22.91 and 20.91 produce masses at fit of 22.25 and 20.12 M_{\odot} , respectively. This mass ratio of 0.904 is consistent with the observational value of 0.910 ± 0.011 (Stickland, Lloyd, & Corcoran 1994), and the masses agree with observation to within the estimated errors ($\pm 0.3 M_{\odot}$).

However, even this loss is still small. A loss of $0.7 M_{\odot}$ is about twice the uncertainty in mass determination, $\pm 0.32 M_{\odot}$. Such a change in mass, since $L \propto M^4$, corresponds to a shift in luminosity of $\Delta \log L \approx 0.05$, to be compared to the observational error in luminosity of $\Delta \log L = 0.1$, which is still larger. This is due to the fact that effective temperature is less well determined than the radius. A concentrated effort to refine the effective temperature determinations for EM Car, V478 Cyg, CW Cep, QX Car, CV Vel, and U Oph would translate directly into much sharper constraints on massive star evolution. Ribas et al. (2000) have revised the effective temperature for QX Car (upward) by twice the quoted error, so that the inferred luminosity increases. Prior to this revision, the fit to QX Car was good ($\chi^2 < 4$). This larger discrepancy for QX Car is in the same sense as noted for the other massive systems; the models are dimmer than the stars. Taking the larger masses from Andersen (1991), with or without mass loss, still gives good fits, and the models are still dimmer than the stars. The result seems robust.

Pachoulakis et al. (1996) have used high resolution spectral images obtained with the International Ultraviolet Explorer (IUE) to study the winds from CW Cephei (HD 218066). They place upper limits on the mass-loss rates of $1.0 \times 10^{-8} M_{\odot} \text{ yr}^{-1}$ for the primary and $0.32 \times 10^{-8} M_{\odot} \text{ yr}^{-1}$ for the secondary. The model masses start at 12.9 and 11.9 and decrease only to 12.8 and 11.88 respectively, to be compared to 12.9 ± 0.1 and $11.9 \pm 0.1 M_{\odot}$ (Stickland, Koch & Pfeiffer 1992). The mass loss predicted by the Kudritzki et al. (1989) theory for our models at the point of minimum error is $0.66 \times 10^{-8} M_{\odot} \text{ yr}^{-1}$ for the primary, and $0.43 \times 10^{-8} M_{\odot} \text{ yr}^{-1}$ for the secondary. If the upper limits were detections, this could be considered good agreement, considering the complexity of the problem of interpreting the system (Pachoulakis et al. 1996). The net loss of mass up to this point is no larger than the error in mass determination, $\pm 0.1 M_{\odot}$. Because the mass loss rate is restricted by these observations to be at or below the value we use, the mass loss process should have no larger effect than we compute. Hence, the remaining discrepancy must come from some other effect.

Table 3 gives the instantaneous mass loss rates from the models, at the point of optimum fit, for the most massive binary systems. At lower masses, the mass loss rates are smaller still. Additional observational data on mass loss for these systems could prove crucial in clarifying the role of mass loss in stellar evolution.

Ribas et al. (2000) estimate ages for EM Car and CW Cep. Their procedure not only gives

ages, but also error estimates for those ages. Our ages agree with theirs to within these errors, even though we use no overshooting and they do. It may be that the convective region in high mass stars is sufficiently large that the gross evolutionary properties of stars on the main sequence are not greatly affected by the overshooting correction. The understanding of the physics of overshooting is still too preliminary to do more than speculate on this issue.

Pols et al. (1997b) find acceptable fits for EM Car, V478 Cyg, CW Cep, QX Car, and U Oph (it is probable that QX Car would not have been a good fit with the revised effective temperatures), but with increasingly lower heavy element abundances with increasing mass. EM Car and V478 Cyg have fits at the limit of the heavy element abundance range. Ribas et al. (2000) find a similar effect: the heavy element abundances of their massive binaries are marginally smaller than those of the less massive ones. Their effect is not quite as obvious as in Pols et al. (1997b), perhaps because Ribas et al. (2000) do not force the helium abundance to correlate with heavy element abundance, and it fluctuates for these systems. The added degree of freedom may allow the fitting procedure to obscure the trend.

This behavior could be interpreted as a galactic evolutionary effect, which would be extremely interesting, but there is another possibility. The problem with the massive models (see Figure 2 and Figure 3) is that they are too dim. Lower heavy element abundance gives higher luminosity because of reduced opacity. The fitting algorithms, having little freedom for mass variation (thanks to the high quality of the data), must find lower heavy element abundance preferable, whether or not the heavy element abundances are actually smaller. More effective mixing, giving larger cores, also results in higher luminosities even if the abundances are unchanged. *It is crucial to obtain spectroscopic information to decide the issue.* Guinan et al. (2000) have recently examined V380 Cyg, which is a binary of disparate masses ($11.1 \pm 0.5 M_{\odot}$ and $6.95 \pm 0.25 M_{\odot}$) and evolutionary state. They conclude that more mixing is needed ($\alpha_{OV} = 0.6 \pm 0.1$). However, this system is complicated. Guinan et al. estimate that the system is approximately ten thousand years from Roche lobe overflow by the primary. Thus, conclusions based on this system should be made with caution.

The overshoot parameter α_{OV} may be a function of mass (at least). Similar behavior can also be seen in Claret & Giménez (1991), which finds different values of the best fit overshoot parameter for five different masses. Alternatively, rotational mixing might be increasingly effective for larger masses. Phenomenological prescriptions are valuable if they capture the essential physics of the phenomena; if fitted parameters turn out to be variable, a new formulation is needed. We have at least three causes for one effect; sorting this out is an interesting theoretical and observational challenge.

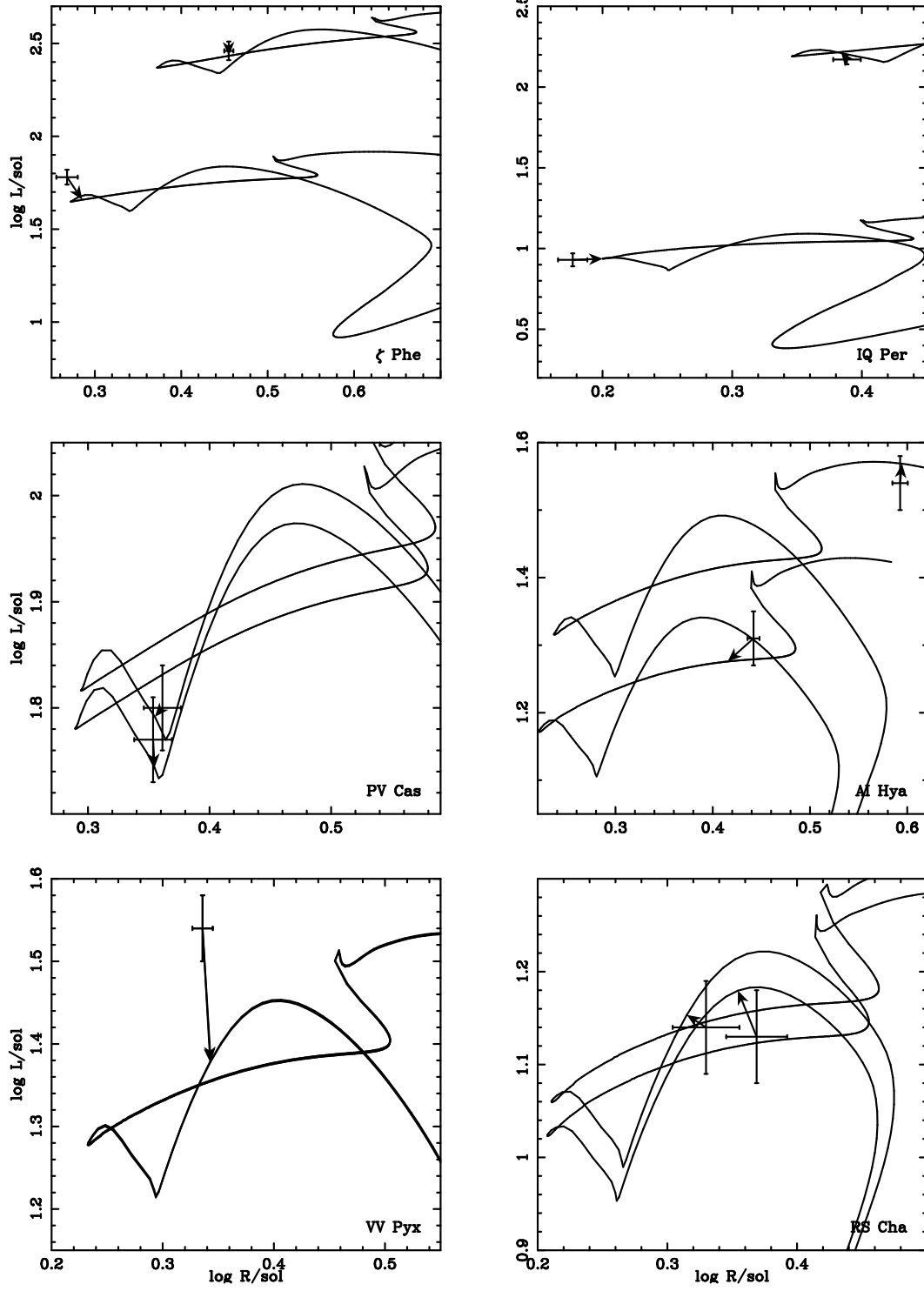


Fig. 6.— Intermediate mass models: ζ Phe, IQ Per, PV Cas, AI Hya, VV Pyx and RS Cha. The masses range from 3.93 to $1.74 M_{\odot}$.

2.3. Intermediate Mass Binaries

Figure 6 shows ζ Phe, IQ Per, PV Cas, AI Hya, VV Pyx, and RS Cha, the group which has some of the most challenging binaries. The masses range from 3.9 to 1.1 M_{\odot} .

Both ζ Phe and IQ Per have a mass ratio significantly different from one: 0.65 and 0.49 respectively. Because the more massive components will evolve more rapidly, common age is a stringent constraint. In both cases, the error is dominated by the less massive component. For ζ Phe, the 2.55 M_{\odot} secondary is brighter than the model; Pols et al. (1997a) have the same problem. Ribas et al. (2000) avoid it by using a lower heavy element abundance (0.013) and a higher helium abundance (0.29). The heavy element abundance might be tested by high resolution spectroscopy. For IQ Per, the 1.74 M_{\odot} secondary is too blue; its evolutionary track never gets so hot. Pols et al. (1997b) attribute the difficulty in fitting ζ Phe and IQ Per to problems in determining T_{eff} of the secondary (Andersen 1991), which is much dimmer because of the large mass ratios of the components.

For ζ Phe and IQ Per, it is clear that much of our “difficulty” is due to the relatively small error bars; see Figure 2. Consequently, small changes may improve the χ^2 significantly, even if they do not correspond to the physics of the system. In the case of IQ Per, use of the Ribas et al. (2000) value of effective temperature improves the fit, compared to Pols et al. (1997a), as does adjustment of the abundances.

AI Hydrae is particularly interesting because the primary is fitted by a model which is swiftly evolving, so that catching it in such a stage is unlikely. Overshoot from the convective core would broaden the main sequence band and increase the age of the fast evolving primary, allowing the possibility of a fit with a more probable, slower evolutionary stage. This is consistent with the conclusions of Pols et al. (1997b), who find that AI Hya is the only binary for which the overshooting models give a greatly improved fit.

Some of the AI Hya behavior can be attributed to heavy element abundance effects. Both members are classified as peculiar metal line stars. The heavy element abundance of this system (from multi-color photometry) is 0.07 (Ribas et al. 2000), which is 3.5 times the value used in the models. The true interior composition cannot be this metal rich. We have examined a sequence which had a heavy element abundance of 0.03 rather than 0.02. This modest change gave a dramatic shift toward lower luminosity ($\Delta \log L \approx 0.06$, which is three times the observational error) and cooler effective temperatures ($\Delta \log T_e \approx 0.027$, which is also three times the observational error). However, if the heavy element abundance were high only near the surface of the star, the opacity effects would produce a shift to the red in the evolutionary tracks, which would bring the models much more in line with the observations.

VV Pyx has almost identical components, so that their coeval origin has almost no effect on the fit. They track the same path at essentially the same time. The fit is simply the point that the observational error box is most closely approached, and should be viewed with caution, especially

as the models give a poor fit.

Only PV Cas and RS Cha have good fits ($\chi^2 < 4$), and they are pre-main sequence (pre-MS). RS Cha has previously been suggested to be in a pre-main sequence stage (Mamajek, Lawson & Feigelson 1999). The pre-MS identification would have important theoretical implications. If true, it implies that the error in the models occurs after the core convection has been established in these stars. In any case, convection is an interesting possible cause for the problem; these binaries have at least one component with convective core burning. PV Cas has sufficiently different masses to require us to examine the pre-MS fit seriously.

2.4. Is PV Cas Pre-Main Sequence?

Questions have been raised about the evolutionary status of PV Cas since Popper (1987). Previous attempts to fit the system to main sequence models (Pols et al. 1997a) have been unsatisfactory, mainly due to a large and irreconcilable age discrepancy between the members. Fitting both components to pre-MS models, however, produces excellent agreement.

To test the case for PV Cas being pre-MS, we looked for other observation clues. The double-lined eclipsing binary system RS Cha was recently found by Mamajek, Lawson & Feigelson (1999, 2000) to be pre-MS. Not only were pre-MS tracks for RS Cha a better fit than post-MS tracks, but two other observations strengthened the argument: (1) RS Cha had several nearby *ROSAT* All-Sky Survey X-ray sources nearby which were found to be very young, low-mass, weak-lined T Tauri stars, and (2) RS Cha’s proper motion matched that of the T Tauri stars, suggesting a genetic tie. PV Cas is at a distance of 660 pc (Popper 1987), and a young stellar aggregate or membership within an OB association could have been previously overlooked.

Searching the Hipparcos and Tycho-2 catalogs, as well as examining PV Cas on the Digitized Sky Survey, we found no evidence for PV Cas being a member of a known OB Association. More massive members of a putative association would be included in the Hipparcos catalog with proper motions similar to that given in the Tycho-2 entry for PV Cas, but none were found. We searched for known groups of young stars with VizieR at CDS: the compilations of OB Associations by Ruprecht, Balazs, & White (1982), Melnick & Efremov (1995), and de Zeeuw et al. (1999), and open clusters by Ruprecht, Balazs, & White (1983) and Lyngå (1987). The only possible known associations that PV Cas could belong to are Cep OB3 (d=840 pc, $\Delta\theta = 4.0^\circ$, $v_R = -23$ km/s) and Cep OB2 (d=615 pc, $\Delta\theta = 9.5^\circ$, $v_R = -21$ km/s), however their projected separations from PV Cas are large (600 pc and 100 pc, respectively), and their average radial velocities are far from Popper’s value for PV Cas ($v_R = -3$ km/s). Hence, PV Cas does not appear to be connected to any known OB Associations or clusters which help us to infer its nature.

The *ROSAT* All-Sky Survey (RASS) Bright Source Catalog (BSC; Voges et al. (1999)) and Faint Source Catalog (FSC; Voges et al. (2000)) were searched to see whether there was any evidence for a clustering of X-ray-emitting T Tauri stars in the vicinity of PV Cas. No concentration of

sources near PV Cas was detected, although the sensitivity of RASS at 660 pc is about $L_x \simeq 10^{31}$ erg s $^{-1}$, corresponding to the very high end of the X-ray luminosity function for T Tauri stars (Feigelson & Montmerle 1999). Only one RASS-BSC source was within 30' (~ 6 pc projected) of PV Cas, but its f_X/f_V ratio was 2 magnitudes too high to be a plausible T Tauri star candidate. The only RASS-FSC source within 30' of PV Cas appeared to be related to a galaxy cluster on the Digitized Sky Survey.

We conclude that we currently have no evidence for a pre-MS aggregate around PV Cas which could strengthen the argument for its pre-MS status. However, the Taurus clouds also are forming low mass pre-MS stars without high mass cluster counterparts.

2.5. Lower Mass Binaries

Figure 7 shows EK Cep, MY Cyg, PV Pup, DM Vir, V1143 Cyg, and UX Men, whose masses range from 2.03 to 1.12 M_\odot . The Ribas et al. (2000) effective temperatures improve the fit for UX Men.

EK Cep has a large mass ratio. The optimum fit occurs as EK Cep B is still on the pre-MS track, in agreement with Martin & Rebolo (1993) and Claret, Giménez, & Martin (1995). We find that the surface abundance of Li⁶ is depleted to about 10^{-4} of its initial value, while Li⁷ is depleted from 1.47×10^{-9} to 0.393×10^{-9} . This corresponds to a depletion of elemental lithium of about 0.57 dex (base 10 logarithm). This is somewhat larger than found by Martin & Rebolo (1993) (0.1 dex), but may be due to differences in the nuclear reaction rates used. In this range, the depletions are almost linear in the net cross section for Li⁷ destruction. A careful analysis with a variety of rates is warranted: Martin & Rebolo (1993) suggest that the observations are in conflict with pre-MS models giving a Li depletion greater than 0.3 dex.

Although EK Cep has a large χ^2 ($\chi^2 = 10.3$) if the radii are used in determining the fitting function, the situation is different for $\log L$ - $\log T_{eff}$, the conventional HR plane. The observational errors are now larger, and the corresponding χ^2 approaches 4. This confirms the importance of using the radii directly as a discriminant (Andersen 1991).

MY Cyg and UX Men are found to be well into main sequence hydrogen burning. MY Cyg is underluminous relative to the models. A higher heavy element abundance would remove the discrepancy; observational tests of this are needed. Pols et al. (1997b) found $Z = 0.024$ and Ribas et al. (2000) found $Z = 0.039$, which are consistent with this suggestion.

PV Pup and V1143 Cyg are on the pre-MS/MS boundary. The fitting procedure chooses the cusp at which the star settles down to main sequence burning. This cusp shifts with small changes in abundance, so these fits would benefit from independent measurement of the abundances in these binaries.

DM Vir has been updated for Latham et al. (1996). Although the changes were small, the new

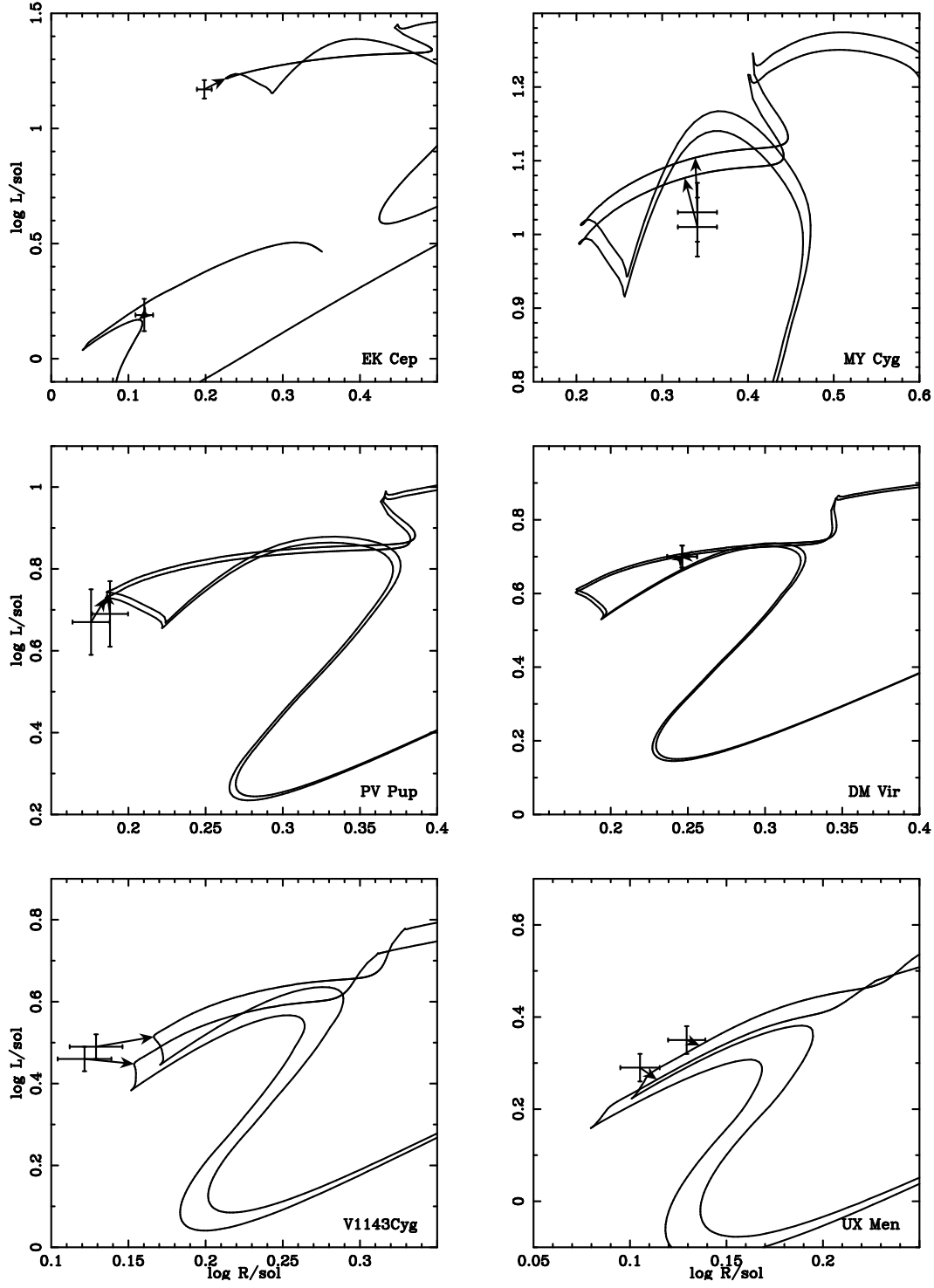


Fig. 7.— Lower mass models: EK Cep, MY Cyg, PV Pup, DM Vir, V1143 Cyg, and UX Men. The masses range from 2.03 to $1.12 M_{\odot}$.

fit is in the middle of main sequence hydrogen burning instead of pre-MS contraction. The track lies well within the error bars; the previous data also had $\chi^2 < 4$, although a much younger age estimate. Because the masses are almost equal, the coeval birth requirement has little effect, and the ages have a corresponding uncertainty.

2.6. Roche Lobes

Observational selection favors binaries with a small separation. In order to determine the true usefulness of these systems as tests of models of single star evolution it is necessary to know to what extent these systems are detached (noninteracting), and how far into the past and the future this condition is satisfied.

In order to answer this question to first order for the systems in our sample, the average Roche lobe radius for each star was calculated using

$$R_{Roche} = \frac{0.49a}{0.6 + q^{-2/3} \ln(1 + q^{1/3})}$$

where a is the binary separation and q is the mass ratio with the star in question in the numerator (Lewin, van Paradijs, & van den Heuvel 1995). This average radius was then compared to the model radii to estimate when each star overflows its Roche lobe. Dynamical evolution of the orbits was not taken into account. None of the models indicated significant mass transfer prior to the ages of the models closest to the observed points since early in the pre-Main Sequence evolution.

Four of the binaries in the sample have at least one member which, according to the model radii, will overflow their Roche lobes when they are between 1.3 and 2 times older than their current age. The results of the Roche lobe comparisons are given in Table 4. All stars labeled “Post” do not exceed their Roche Lobe radius until well into their post-main sequence evolution. Two stars are in contact early in the pre-main sequence evolution (EK Cep B and MY Cyg A). The times given for these stars correspond to when they contract below the critical radius and mass transfer ends. These numbers should be taken as a rough guideline at best, since the dynamical evolution of protostars is undoubtedly more complex than the simple algorithm used here. The models corresponding to the primaries EM Car and V478 Cyg exceed their Roche lobe radii in less than 3×10^6 years.

These values are approximate in that dynamical evolution is not taken into account, the model radii do not match exactly the observed radii, and an approximate Roche lobe geometry was used to facilitate comparison to the spherically symmetric models.

3. APSIDAL MOTION

Apsidal motion in binaries allows us to infer constraints on the internal mass distributions (Schwarzschild 1957). Apsidal motion, that is, rotation of the orientation of the orbital ellipse relative to an inertial frame, does not occur for binary orbits of point particles interacting by Newtonian gravity. Levi-Civita (1937) showed that the general relativistic expression for the periastron shift of a double star is the same as for the perihelion shift of Mercury. Following Weinberg (1972) (see pages 194-7), the shift is

$$(P/U)_{GR} = 3G(M_A + M_B)P/a(1 - e^2)c^2, \quad (2)$$

where c is the speed of light and G the gravitational constant. Using units of solar masses and radii, and with the period P in days, this dimensionless number becomes

$$(P/U)_{GR} = 6.36 \times 10^{-6}(M_A + M_B)P/a(1 - e^2), \quad (3)$$

apsidal orbits per orbit. Tests of general relativity have reached high precision (Will 1998); the perihelion shift has now been tested to about 3×10^{-3} . There has been some controversy as to a possible breakdown of general relativity because of a discrepancy between observations and predictions of the apsidal motion of some systems. This has been clarified by Claret (see Claret (1997, 1998) for a recent discussion), who pointed out errors in theoretical models and difficulties in observations, especially for systems whose apsidal periods are too long for much to be measured with modern equipment. We adopt the point of view that general relativity is better tested than subtleties in the evolution of binary stars, and ascribe errors to other causes (tidal effects not included, rotational effects, and systematic errors in observational interpretation, for example).

Tides induced by each companion give an additional interaction which is not purely inverse square in the separation and cause apsidal motion. Quataert, Kumar & On (1996) have discussed the validity of the classical formula, which we use,

$$(P/U)_{CL} = (15/a^5)[k_1 R_1^5 M_2/M_1 + k_2 R_2^5 M_1/M_2]f(e), \quad (4)$$

where P is the period of the orbit, U the period of apsidal motion, M_i the mass and R_i the radius of the star i , and

$$f(e) = (1 + \frac{3}{2}e^2 + \frac{1}{8}e^4)/(1 - e^2)^5, \quad (5)$$

where e is the eccentricity of the orbit. The separation of the pair in solar radii is

$$a = 4.207 P^{\frac{2}{3}}(M_1 + M_2)^{\frac{1}{3}}, \quad (6)$$

if the period P is measured in days and the masses in solar units. The classical apsidal motion formula gives accurate results when the periods of the low-order quadrupole g , f and p -modes are smaller than the periastron passage time by a factor of about 10 or more (Quataert, Kumar & On 1996). For EM Car, the lowest order pulsational mode of the primary has a period of 0.324

days compared with the orbital period of 3.414 days and an eccentricity of 0.0120 ± 5 , so that this condition is just satisfied.

If we assume that the observed apsidal motion is due only to these two effects, classical simple tides and general relativity, we have

$$(P/U)_{OBS} - (P/U)_{GR} = (P/U)_{CL}. \quad (7)$$

We use the products $k_i R_i^5$ directly for greater precision, but quote the apsidal constants k_i for comparison. Petrova (1995) has pointed out that accuracy problems may exist because the relevant parameter is $k_i R^5$, where k_i is the apsidal constant and R is the stellar radius, not just k_i alone.

Figure 8 shows the integrand of the apsidal constant, which approaches an asymptotic value as the integration exceeds about 0.7 of the radius. Inner regions contribute little because of their small radii; outer regions have little mass. The change from the interior (Henye) integration to envelope integration occurs around $r/R = 0.5$, and is visible in the change in the density of points. At the join, the temperature is about $T \approx 6 \times 10^6$ K, and the density $\rho \approx 2.0 \times 10^{-2}$ gcm $^{-3}$. This temperature is about ten times the value attained in the early opacity experiments (Perry et al. 1991, 1996) on the NOVA laser, and is about half the goal for the National Ignition Facility (NIF). For such main sequence (and pre-main sequence) stars, the apsidal constants are most sensitive to the range of density and temperature which is directly accessed by high energy density laser experiments (see Remington et al. (1999) and discussion above). In this range, the new opacities show significant deviation from those previously used in astrophysics (Rogers & Iglesias 1992; Iglesias & Rogers 1996).

The Petrova & Orlov (1999) catalog contains orbital elements for 128 binaries, including most (11 of 18) of the binaries in our list. Table 5 gives apsidal constants k_i , as well as the observed and predicted ratios of P/U . Given the significant improvement in the opacities, a critical re-examination of these data seems warranted.

Figure 9 shows the dimensionless rate of apsidal motion, $(P/U)_{CL} = (P/U)_{OBS} - (P/U)_{GR}$, which would be due to classical apsidal motion, plotted versus log of half the total binary mass. P is the orbital period and U the apsidal period. The observational data (corrected for general relativity) are shown as diamonds, with vertical error bars. The model predictions are shown as solid squares ($\chi^2 < 4$) for the best fits, open triangles for $4 < \chi^2 < 16$, and crosses for $\chi^2 > 16$. The massive binaries with good fits (EM Car, V478 Cyg, and CW Cep; $(M_A + M_B)/2 > 10M_\odot$) have predicted apsidal motion in excess of that observed, and QX Car also follows that trend. These models are not as centrally condensed as the stars. This may be related to the underluminosity of these models found above. Additional mixing would give more massive, convective cores, which would result in both greater luminosity and more centrally condensed structure.

Of the lower mass binaries with measured apsidal motion, only PV Cas has a good fit model. Its predicted apsidal motion is also larger than that observed (the stars are more centrally condensed). The other binaries need better fitting models before the tests can be convincing. Note that at the

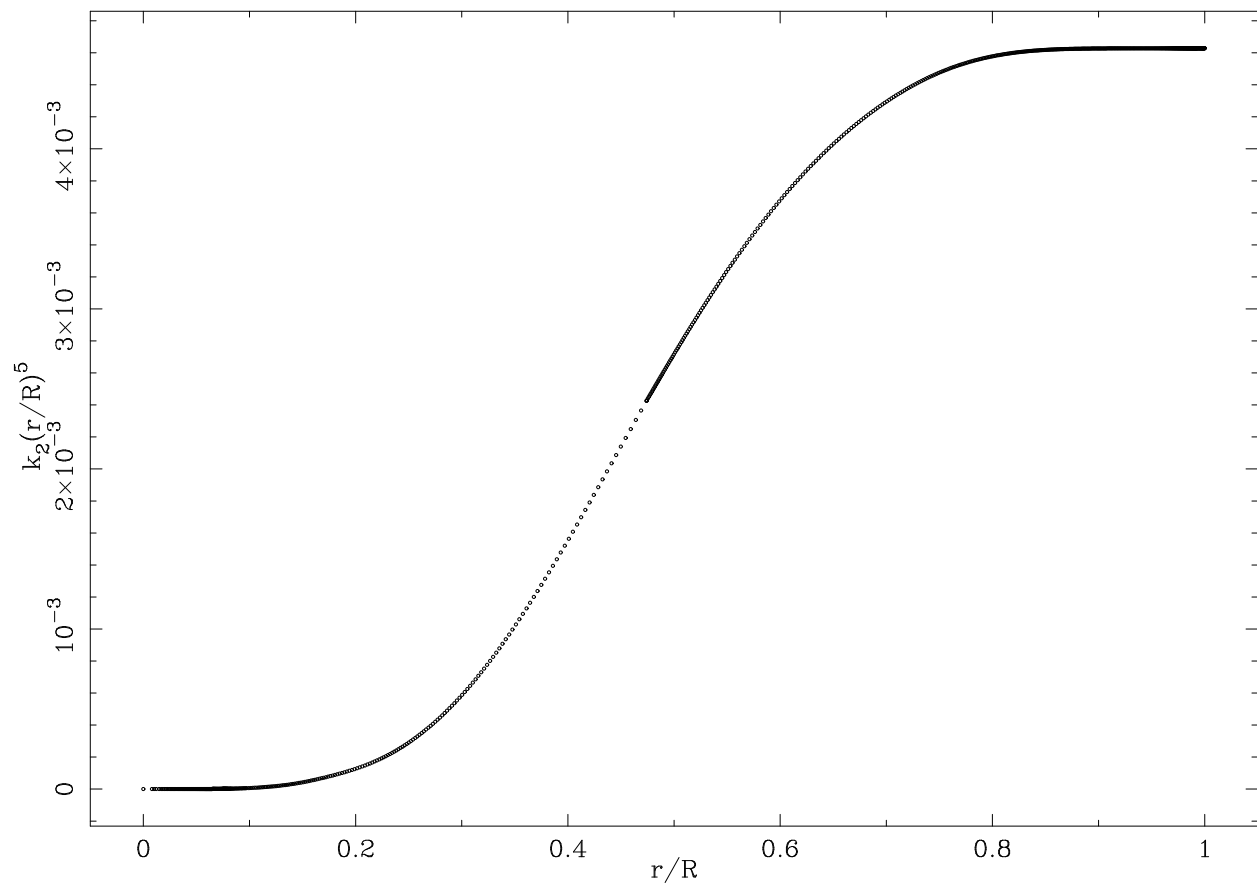


Fig. 8.— Apsidal Constant integrand for EM Car primary.

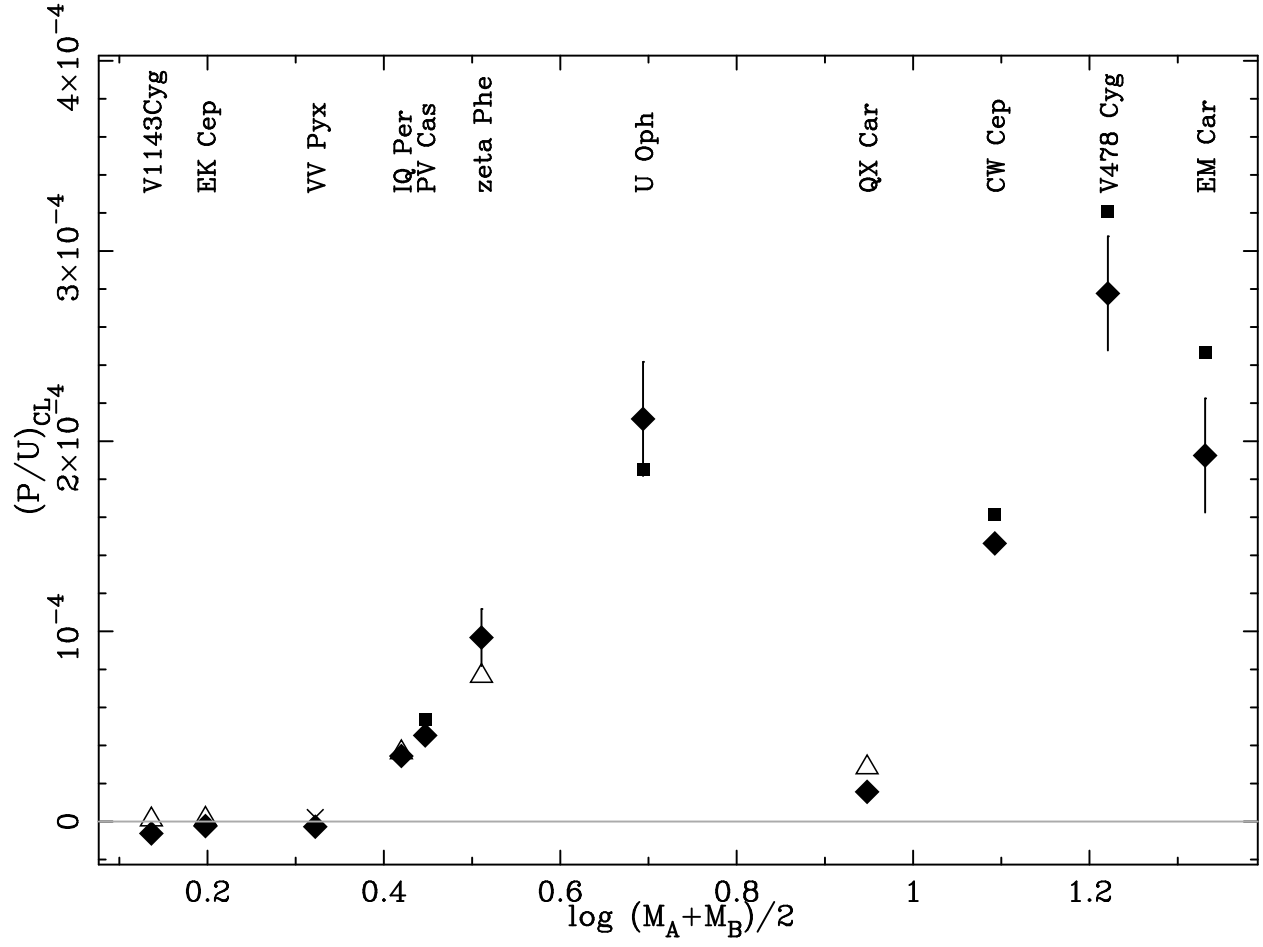


Fig. 9.— Classical apsidal motion versus mean mass, for our binaries with measured apsidal motion. $(P/U)_{CL} = (P/U)_{OBS} - (P/U)_{GR}$ is assumed.

lowest tick mark in Figure 9, the apsidal period is measured in centuries.

Claret & Giménez (1993) have shown that inclusion of (a) overshooting, (b) variation in heavy element abundance, and (c) rotation can produce models consistent with the apsidal data; see also (Claret 1999). This represents good progress toward establishing the apsidal motion data as a useful test of stellar evolution. Our results, while not based upon identical assumptions, are consistent. The challenge is that of correctly determining the relative importance of the several different small effects which can give consistency with the observations.

4. CONCLUSIONS

Standard stellar evolution, without embellishments such as overshooting and rotation, does fairly well on these quantitative tests. While clear discrepancies exist, they are relatively subtle. This makes it difficult to uniquely identify exactly which additional physics is needed. We find a detailed consistency with similar calculations by Pols et al. (1997b) and Ribas et al. (2000). It is important to test observationally the abundance variations implied by χ^2 optimization, as such procedures may hide missing physics in parameter variation. Laser experiments now explore the regions of temperature and density which are relevant not only to conventional stellar evolution, but also to apsidal motion tests.

Massive stars require more mixing than given by standard stellar evolution, and probably more than the prescriptions for overshooting used by Pols et al. (1997b) and Ribas et al. (2000). Rotational mixing, overshooting which is mass dependent, or something else is needed. Our mass loss prescription is near the observational upper limit, so that additional mass loss is an unlikely solution.

Lower mass stars with convective cores are not well fit by standard stellar evolution. Again, additional mixing is a promising answer. Several of these binaries seem to be pre-main sequence; this will allow some interesting tests of depletion of light nuclei and the mixing processes.

We find two serious challenges: (1) disentangling conflicting solutions of the relatively subtle discrepancies, and (2) controlling shifts in the observational “target areas” due to systematic errors, which seem to be larger than the statistical errors. Improved determinations of effective temperature, and of heavy element abundances (e.g., $[\text{Fe}/\text{H}]$), would greatly improve these tests.

Stimulating discussions with Brigitta Nordstrom and Johannes Andersen are gratefully acknowledged. Special thanks are due to Marcel Arnould, Shimon Asida, John Bahcall, Audra Baleisis, Al Cameron, Joergen Christensen-Dalgaard, Paul Drake, Rolf Kudritzki, Robert Kurucz, T. J. Pearson, Ted Perry, Thomas Rauscher, Marc Rayet, Bruce Remington, Friedel Thielemann, Frank Timmes, and Cliff Will, whose work and/or advice contributed to aspects of this paper. This work was supported in part by DOE, grant number DE-FG03-98DP00214/A001, and a subcontract

from ASCI Flash Center at U. of Chicago.

REFERENCES

- Anders, E. & Grevesse, N. 1989, *Geochim. Cosmochim. Acta* 53, 197
- Andersen, J., Nordström, B., & Clausen, J. V., 1990, *ApJ*, 363, 33
- Andersen, J. 1991, *A&A Rev.*, 3, 91
- Angulo, C., 1999, *Nuclear Phys. A* 656, 3
- Arnett, D. 1996, *Supernovae and Nucleosynthesis*, Princeton University Press.
- Asida, S.M., & Arnett, D. 2000 *ApJ*, 545, 435
- Asida, S., 1998, *ApJ*, 528, 896
- Bahcall, J. N. & Pinsonneault, M. H. 1998, private communication
- Bodenheimer, P., 1965 *ApJ*, 142, 451
- Bressan, A., Fagotto, F., Bertelli, G., & Chiosi, C., 1993, *A&AS*, 100, 647
- Canuto, V. M., & Mazzitelli, I., 1991, *ApJ*, 370, 295
- Canuto, V. M., & Mazzitelli, I., 1991, *ApJ*, 389, 724
- Caughlan, G., & Fowler, W. A., 1988, *Atomic and Nuclear Data Tables*, 40, 283
- Christensen-Dalsgaard, J. 2000, private communication
- Claret, A., 1995, *A&AS*, 109, 441
- Claret, A., 1997, *A&A*, 327, 11
- Claret, A., 1997, *A&AS*, 125, 439
- Claret, A., 1998, *A&A*, 330, 533
- Claret, A., 1999, *A&A*, 350, 56
- Claret, A., & Giménez, 1991, *A&A*, 249, 319
- Claret, A., & Giménez, 1993, *A&A*, 277, 487
- Claret, A., & Giménez, 1995, *A&AS*, 114, 549
- Claret, A., & Giménez, 1998, *A&AS*, 133, 123

- Claret, A., Giménez, & Martin, E. L., 1995, *A&A*, 302, 741
- Däppen, W., & Nayfonov, A., 2000, *ApJS*, 127, 287
- Davidson, S. J., Nazir, K., et al., 2000, *J. Quant. Spec. Radiat. Transf.*, 65, 151
- de Jager, C., Nieuwenhuijzen, H., & van der Hucht, K. A. 1988, *A&A*, 173, 293
- de Zeeuw, T., Hoogerwerf, R., de Bruijne, J. H. J., Brown, A. G. a., & Blaauw, A., 1999, *AJ*, 117, 354
- Dominguez, I., Chieffi, A., Limongi, M., & Straniero, O., 1999, *ApJ*, 524, 226
- Elliott, J. R., Miesch, M. S., & Toomre, J., 2000, *ApJ*, 533, 546
- Feigelson, E. D., & Montmerle, T., 1999, *ARA&A*, 37, 363
- Gimenez, A., Clausen, J. V., & Jensen, K. S., 1986, *A&A*, 159, 157
- Guinan, E. F., Ribas, I., Fitzpatrick, E. L., Giménez, Jordi, C., McCook, G. P., & Popper, D. M., 2000, *ApJ*, 544, 404
- Heney, L. G., Wilets, L., Böhm, K. H., LeLevier, Robert, & Levee, R. D., 1959, *ApJ*, 129, 628
- Iglesias, C., Wilson, B. G., et al., 1995 *ApJ*, 445, 855
- Iglesias, C. & Rogers, F. J. 1996 *ApJ*, 464, 943
- Kippenhahn, R., & Weigert, A., 1990, *Stellar Structure and Evolution*, Springer-Verlag, Berlin
- Kudritzki, R. P., Pauldrach, A., Puls, J., Abbott, & D. C. 1989 *A&A*, 219, 205
- Kurucz, R. L., 1991, in *Stellar Atmospheres: Beyond Classical Models*, NATO ASI Series C, vol. 341
- Latham, D. W., Nordström, B., Andersen, J., Torres, G., Stefanik, R. P., Thaller, M., & Bester, M. J., 1996, *A&A*, 314, 864
- Levi-Civita, T., 1937, *Am. J. Math.*, 59, 225
- Lewin, W. H. G., van Paradijs, J., & van den Heuvel, P. J. 1995, *X-Ray Binaries*, Cambridge University Press, p.469
- Lyngå, G., 1987, *Catalogue of Open Cluster Data*, 5th. ed., Lund Observatory
- Maeder, A., 1975, *A&A*, 40, 303
- Martin, E. L., & Rebolo, R., 1993, *A&A*, 274, 274
- Mamajek, E. E., Lawson, W. A., & Feigelson, E. D., 1999, *ApJ*, 516, L77

- Mamajek, E. E., Lawson, W. A., & Feigelson, E. D., 2000, *ApJ*, 544, 356
- Melnick, A. M., & Efremov, Yu. N., 1995, *Proc. Astron. Zhurnal*, 21, 13
- Meynet, G. & Maeder, A., 2000, *A&A*, 361, 101
- Mostovych, A. N., Chan, L. Y., et al., 1995, *Phys. Rev. Lett.*, 75, 1530
- Norberg, P., & Maeder, A., 2000, *A&A*, 359, 1025
- Pachoulakis, I., Pfeiffer, R. J., Koch, R. H., & Strickland, D. J., 1996, *The Observatory*, 116, 89
- Perry, T. S., Davidson, S. J., et al., 1991, *Phys. Rev. Lett.*, 67, 3784
- Perry, T. S., Springer, P. T., et al., 1996, *Phys. Rev. E*, 54, 5617
- Petrova, A. V., 1995, *AZh*, 72, 937
- Petrova, A. V. & Orlov, V. V., 1999, *AJ*, 117, 587
- Pols, O. R., Tout, C. A., Eggleton, P. P., & Han, Z., 1997, *MNRAS*, 274, 964
- Pols, O. R., Tout, C. A., Schröder, K-P., Eggleton, P. P., & Manners, J., 1997, *MNRAS*, 289, 869
- Popper, D. M., 1987, *AJ*, 93, 672
- Porter, D. H., & Woodward, P. R., 1994, *ApJS*, 93, 309
- Porter, D. H., & Woodward, P. R., 2000, *ApJS*, 127, 159
- Press, W. H., Teukolsky, S. A., Vetterling, W. T., & Flannery, B. P., 1992, *Numerical Recipes in FORTRAN*, Second Edition, University Press: Cambridge,
- Quataert, E. J., Kumar, P., & On, Chi, 1996, *ApJ*, 463, 284
- Rauscher, T., & Thielemann, K.-F., 2000, *Atomic Data Nuclear Data Tables*, 75, 1
- Remington, B. A., Arnett, D., Drake, R. P., & Takabe, H. 1999, *Science*, 284, 1488
- Ribas, I., Jordi, C., Torra, J., & Giménez, Á., 2000, *MNRAS*, 313, 99
- Rogers, F. J., & Iglesias, C. A., 1992, *ApJS*, 79, 507
- Rosenthal, C. S., Christensen-Dalsgaard, J., Nordlund, Aa., Stein, R. F., & Trampedach, R., 1999, *A&A*, 351, 689
- Ruprecht, J., Balazs, B., & White, R. E., 1982, *Bull. Int. Centre Donnees Stellaires*, 22, 132
- Ruprecht, J., Balazs, B., & White, R. E., 1983, *Soviet Astronomy*, 27, 358

- Schaller, G., Schaerer, D., Meynet, G., & Maeder, A., 1992, *A&AS*, 96, 269
- Schröder, K-P., Pols, O. R., & Eggleton, P. P., 1997, *MNRAS*, 285, 696
- Schwarzschild, M., 1957, *Structure and Evolution of the Stars*, Princeton University Press, Princeton, New Jersey, p. 146
- Springer, P. T., Fields, D. J., et al., 1992, *Phys. Rev. Lett.*, 69, 3735
- Stickland, D. J., Koch, R. H., & Pfeiffer, R. J., 1992, *Obs.*, 112, 277
- Stickland, D. J., Lloyd, C., Corcoran, M. F., 1994, *Obs.*, 114, 284
- Thielemann, F.-K., Arnould, M., & Truran, J. W., 1988, in *Advances in Nuclear Astrophysics*, eds. E. Vangioni-Flam, et al, Editions Frontiers: Gif sur Yvette, and private communication from FKT
- Timmes, F. & Arnett, D., 1999, *ApJS*, 125, 277
- Voges, W., et al., 1999, *A&A*, 349, 389
- Voges, W., et al., 2000, *ROSAT All-Sky Survey Faint Source Catalog (RASS-FSC)*, Max-Planck-Institut für Extraterrestrische Physik, Garching
- Wasaburo, U., Kiguchi, M., & Kitamura, M. 1994, *PASJ*, 46, 613
- Weinberg, S., 1972, *Gravitation and Cosmology*, John Wiley & Sons, New York
- Will, C. M., 1998, *The Confrontation between General Relativity and Experiment: A 1998 Update*; see also www.livingreviews.org/Articles/ for an upcoming review

Fig. 1.— χ^2 for selected binaries.

Fig. 2.— Goodness of fit vectors for selected binaries.

Fig. 3.— Luminosity differences.

Fig. 4.— Radius differences.

Fig. 5.— Massive models.

Fig. 6.— Intermediate mass models.

Fig. 7.— Lower mass models.

Fig. 8.— Apsidal Constant integrand for EM Car primary.

Fig. 9.— Apsidal motion versus mass.

Table 1. Observed parameters for selected binary systems.^a

System	P(d)	Star	Spect.	Mass/ M_{\odot}	Radius/ R_{\odot}	$\log g(\text{cm/s}^2)$	$\log T_e(\text{K})$	$\log L/L_{\odot}$
EM Car	3.41	A	O8V	22.3 ± 0.3^b	9.34 ± 0.17	3.864 ± 0.017^b	4.531 ± 0.026	5.02 ± 0.10
HD97484	...	B	O8V	20.3 ± 0.3^b	8.33 ± 0.14	3.905 ± 0.016^b	4.531 ± 0.026	4.92 ± 0.10
V478 Cyg	2.88	A	O9.5V	16.67 ± 0.45	7.423 ± 0.079	3.919 ± 0.015	4.484 ± 0.015	4.63 ± 0.06
HD193611	...	B	O9.5V	16.31 ± 0.35	7.423 ± 0.079	3.909 ± 0.013	4.485 ± 0.015	4.63 ± 0.06
CW Cep	2.73	A	B0.5V	12.9 ± 0.1^c	5.685 ± 0.130	4.039 ± 0.024^c	4.449 ± 0.011^d	4.26 ± 0.06^e
HD218066	...	B	B0.5V	11.9 ± 0.1^c	5.177 ± 0.129	4.086 ± 0.024^c	4.439 ± 0.011^d	4.14 ± 0.07^e
QX Car	4.48	A	B2V	9.267 ± 0.122	4.289 ± 0.091	4.140 ± 0.020	4.395 ± 0.009^d	3.80 ± 0.04^e
HD86118	...	B	B2V	8.480 ± 0.122	4.051 ± 0.091	4.151 ± 0.021	4.376 ± 0.010^d	3.67 ± 0.04^e
CV Vel	6.89	A	B2.5V	6.100 ± 0.044	4.087 ± 0.036	4.000 ± 0.008	4.254 ± 0.012^d	3.19 ± 0.05
HD77464	...	B	B2.5V	5.996 ± 0.035	3.948 ± 0.036	4.023 ± 0.008	4.251 ± 0.012^d	3.15 ± 0.05
U Oph	1.68	A	B5V	5.198 ± 0.113	3.438 ± 0.044	4.081 ± 0.015	4.211 ± 0.015^d	2.87 ± 0.08^e
HD156247	...	B	B6V	4.683 ± 0.090	3.005 ± 0.055	4.153 ± 0.018	4.188 ± 0.015^d	2.66 ± 0.08^e
ζ Phe	1.67	A	B6V	3.930 ± 0.045	2.851 ± 0.015	4.122 ± 0.009	4.149 ± 0.010^d	2.46 ± 0.04^e
HD6882	...	B	B8V	2.551 ± 0.026	1.853 ± 0.023	4.309 ± 0.012	4.072 ± 0.007^d	1.78 ± 0.04^e
IQ Per	1.74	A	B8V	3.521 ± 0.067	2.446 ± 0.026	4.208 ± 0.019	4.111 ± 0.008^d	2.17 ± 0.03^e
HD24909	...	B	A6V	1.737 ± 0.031	1.503 ± 0.017	4.323 ± 0.013	3.906 ± 0.008^d	0.93 ± 0.04^e
PV Cas	1.75	A	B9.5V	2.815 ± 0.050^d	2.297 ± 0.035^d	4.165 ± 0.016^d	4.032 ± 0.010^d	1.80 ± 0.04^e
HD240208	...	B	B9.5V	2.756 ± 0.054^d	2.257 ± 0.035^d	4.171 ± 0.016^d	4.027 ± 0.010^d	1.77 ± 0.04^e
AI Hya	8.29	A	F2m	2.145 ± 0.038	3.914 ± 0.031	3.584 ± 0.011	3.851 ± 0.009^d	1.54 ± 0.02^e
+0°2259	...	B	F0V	1.978 ± 0.036	2.766 ± 0.017	3.850 ± 0.010	3.869 ± 0.009^d	1.31 ± 0.02^e
VV Pyx	4.60	A	A1V	2.101 ± 0.022	2.167 ± 0.020	4.089 ± 0.009	3.979 ± 0.009^d	1.54 ± 0.04
HD71581	...	B	A1V	2.099 ± 0.019	2.167 ± 0.020	4.088 ± 0.009	3.979 ± 0.009^d	1.54 ± 0.04
RS Cha	1.67	A	A8V	1.858 ± 0.016	2.137 ± 0.055	4.047 ± 0.023	3.883 ± 0.010^d	1.14 ± 0.05^e
HD75747	...	B	A8V	1.821 ± 0.018	2.338 ± 0.055	3.961 ± 0.021	3.859 ± 0.010^d	1.13 ± 0.05^e
EK Cep	4.43	A	A1.5V	2.029 ± 0.023	1.579 ± 0.007	4.349 ± 0.010	3.954 ± 0.010	1.17 ± 0.04
HD206821	...	B	G5Vp	1.124 ± 0.012	1.320 ± 0.015	4.25 ± 0.010	3.756 ± 0.015	0.19 ± 0.07
MY Cyg	4.01	A	F0m	1.811 ± 0.030	2.193 ± 0.050	4.007 ± 0.021	3.850 ± 0.010^d	1.03 ± 0.04^e
HD193637	...	B	F0m	1.786 ± 0.025	2.193 ± 0.050	4.014 ± 0.021	3.846 ± 0.010^d	1.02 ± 0.04^e
PV Pup	1.66	A	A8V	1.565 ± 0.011	1.542 ± 0.018	4.257 ± 0.010	3.840 ± 0.019	0.69 ± 0.08
HD62863	...	B	A8V	1.554 ± 0.013	1.499 ± 0.018	4.278 ± 0.011	3.841 ± 0.019	0.67 ± 0.08
DM Vir ^f	4.67	A	F7V	1.454 ± 0.008	1.763 ± 0.017	4.108 ± 0.009	3.813 ± 0.007	0.70 ± 0.03
HD123423 ^f	...	B	F7V	1.448 ± 0.008	1.763 ± 0.017	4.106 ± 0.009	3.813 ± 0.020	0.70 ± 0.03
V1143 Cyg	7.64	A	F5V	1.391 ± 0.016	1.346 ± 0.023	4.323 ± 0.016	3.820 ± 0.007^d	0.49 ± 0.03^e
HD185912	...	B	F5V	1.347 ± 0.013	1.323 ± 0.023	4.324 ± 0.016	3.816 ± 0.007^d	0.46 ± 0.03^e
UX Men	4.18	A	F8V	1.238 ± 0.006	1.347 ± 0.013	4.272 ± 0.009	3.785 ± 0.007^d	0.35 ± 0.03^e
HD37513	...	B	F8V	1.198 ± 0.007	1.274 ± 0.013	4.306 ± 0.009	3.781 ± 0.007^d	0.29 ± 0.03^e

^aDetailed references and discussion may be found in (Andersen 1991).

^bStickland, Lloyd, & Corcoran (1994).

^cStickland, Koch & Pfeiffer (1992).

^dRibas et al. (2000).

^eAdjusted here.

^fLatham et al. (1996).

Table 2. Parameters for selected binary systems.

System	Star	Mass	$\log R/R_{\odot}$	$\log T_e$	$\log L$	$\log \text{Age (yr)}$	χ^2
EM Car	A	22.89	0.972	4.509	4.933	6.666	1.67
HD97484	B	21.43	0.937	4.504	4.843	6.668	
V478 Cyg	A	16.67	0.879	4.464	4.566	6.807	2.67
HD193611	B	16.31	0.866	4.462	4.530	6.808	
CW Cep	A	13.52	0.766	4.440	4.245	6.788	2.39
HD218066	B	12.08	0.720	4.421	4.075	6.798	
QX Car	A	9.267	0.649	4.362	3.698	6.986	11.3
HD86118	B	8.480	0.611	4.343	3.544	7.000	
CV Vel	A	6.100	0.614	4.231	3.103	7.604	1.30
HD77464	B	5.996	0.603	4.228	3.070	7.607	
U Oph	A	5.198	0.538	4.198	2.820	7.687	0.43
HD156247	B	4.683	0.480	4.177	2.623	7.699	
ζ Phe	A	3.930	0.457	4.136	2.409	7.831	11.4
HD6882	B	2.551	0.283	4.028	1.633	7.836	
IQ Per	A	3.521	0.380	4.119	2.189	7.656	6.92
HD24909	B	1.737	0.195	3.891	0.906	7.688	
PV Cas	A	2.827	0.362	4.015	1.736	6.576	1.12
HD240208	B	2.768	0.351	4.011	1.698	6.577	
AI Hya	A	2.145	0.539	3.866	1.494	9.023	21.4
+0°2259	B	1.978	0.395	3.865	1.204	9.025	
VV Pyx	A	2.101	0.349	3.920	1.331	6.850	32.2
HD71581	B	2.099	0.350	3.920	1.330	6.850	
RS Cha	A	1.858	0.324	3.893	1.174	6.925	1.57
HD75747	B	1.821	0.363	3.876	1.183	6.928	
EK Cep	A	2.029	0.228	3.952	1.217	7.429	10.3
HD206821	B	1.124	0.086	3.761	0.166	7.432	
MY Cyg	A	1.811	0.347	3.851	1.052	9.117	6.69
HD193637	B	1.786	0.329	3.853	1.025	9.121	
PV Pup	A	1.565	0.183	3.858	0.750	7.980	1.66
HD62863	B	1.554	0.182	3.855	0.738	8.101	
DM Vir	A	1.460	0.241	3.802	0.639	7.177	0.15
HD123423	B	1.454	0.240	3.800	0.633	7.180	
V1143 Cyg	A	1.391	0.169	3.789	0.447	7.323	9.13
HD185912	B	1.347	0.151	3.783	0.388	7.327	
UX Men	A	1.238	0.140	3.781	0.356	9.266	2.31
HD37513	B	1.198	0.119	3.773	0.283	9.303	

Table 3. Predicted instantaneous mass loss rates.

System	Star	Mass	Mass Loss Rate ^a
EM Car	A	22.35	1.82×10^{-7}
	B	20.51	1.17×10^{-7}
V478 Cyg	A	16.78	2.50×10^{-8}
	B	16.47	2.28×10^{-8}
CW Cep ^b	A	12.87	0.66×10^{-8}
	B	11.88	0.43×10^{-8}
QX Car	A	9.257	1.31×10^{-9}
	B	8.479	6.32×10^{-11}

^aPredicted instantaneous mass loss rate in M_{\odot}/yr .

^bFor IUE upper limit, see Pachoulakis et al. (1996).

Table 4. Roche lobe parameters for selected binary systems.

System	Star	Mass	a/R_{\odot}	e	R/R_{\odot}	R_{roche}/R_{\odot}	log Age (yr)	log Age(over)
EM Car	A	22.89	33.75	0.0120 ± 5	9.34	12.9	6.666	6.795
	B	21.43			8.33	12.6	6.668	6.832
V478 Cyg	A	16.67	27.31	0.019 ± 2	7.42	10.5	6.807	6.949
	B	16.31			7.42	10.2	6.808	6.965
CW Cep	A	13.52	24.22	0.0293 ± 6	5.68	9.33	6.788	7.085
	B	12.08			5.18	8.91	6.798	7.168
QX Car	A	9.267	29.82	0.0278 ± 3	4.29	11.5	6.986	Post
	B	8.480			4.05	11.0	7.000	Post
CV Vel	A	6.100	34.97	$< 4 \times 10^{-3}$	4.09	17.0	7.604	Post
	B	5.996			3.95	13.2	7.607	Post
U Oph	A	5.198	12.76	0.0031 ± 2	3.44	4.90	7.687	7.910
	B	4.683			3.01	4.68	7.689	8.030
ζ Phe	A	3.930	11.04	0.0113 ± 20	2.85	4.57	7.831	8.276
	B	2.551			1.85	3.80	7.836	8.797
IQ Per	A	3.521	10.58	0.076 ± 4	2.45	4.68	7.656	8.405
	B	1.737			1.50	3.39	7.688	Post
PV Cas	A	2.827	10.85	0.032 ± 1	2.30	4.07	6.576	8.669
	B	2.768			2.26	4.07	6.577	8.697
AI Hya	A	2.145	27.63	0.230 ± 2	3.91	10.7	9.023	Post
	B	1.978			2.77	10.2	9.025	Post
VV Pyx	A	2.101	18.77	0.0956 ± 9	2.17	7.08	6.850	9.066
	B	2.099			2.17	7.08	6.850	Post
RS Cha	A	1.858	9.14	0.030 ± 15	2.14	3.47	6.925	Post
	B	1.821			2.34	3.47	6.928	Post
EK Cep	A	2.029	16.64	0.190 ± 3	1.58	7.08	7.429	Post
	B	1.124			1.32	5.50	7.432	5.669
MY Cyg	A	1.811	16.27		2.19	6.17	9.117	5.646
	B	1.786			2.19	6.17	9.121	Post
PV Pup	A	1.565	8.62	0.050 ± 1	1.54	6.17	7.980	Post
	B	1.554			1.50	6.17	8.101	Post
DM Vir	A	1.460	16.79	$< 10^{-4}$	1.73	6.31	7.177	Post
	B	1.454			1.73	6.31	7.180	Post
V1143 Cyg	A	1.391	22.83	0.540 ± 5	1.35	8.71	7.323	Post
	B	1.347			1.32	8.51	7.327	Post
UX Men	A	1.238	14.69	0.015 ± 17	1.35	5.62	9.266	Post
	B	1.198			1.27	5.50	9.303	Post

Table 5. Apsidal comparisons for selected binary systems.

System	Star	Mass	$-\log k_i$	$(k_2 R^5)^a$	P/U_{CL}^b	P/U_{GR}^b	$P/U_{\text{CL+GR}}^b$	P/U_{OBS}^b
EM Car	A	22.35	2.240	437.9	2.46	0.275	2.74	2.2 ± 0.3
	B	20.51	2.180	290.8				
V478 Cyg	A	16.78	2.185	169.8	3.21	0.223	3.43	3.0 ± 0.3
	B	16.47	2.175	154.7				
CW Cep	A	12.87	2.106	52.86	1.61	0.178	1.79	1.640 ± 0.014
	B	11.88	2.090	37.23				
QX Car	A	9.257	2.122	16.20	0.171	0.170	0.341	0.340 ± 0.006
	B	8.479	2.117	10.96				
U Oph	A	5.198	2.266	2.721	1.85	0.0827	1.93	2.2 ± 0.3
	B	4.683	2.256	1.549				
ζ Phe	A	3.930	2.308	0.9756	0.765	0.0624	0.827	1.03 ± 0.15
	B	2.551	2.333	0.1315				
IQ Per	A	3.521	2.278	0.4619	0.363	0.0553	0.418	0.40 ± 0.03
	B	1.737	2.416	0.0401				
PV Cas	A	2.815	2.321	0.2647	0.538	0.0572	0.597	0.510 ± 0.011
	B	2.756	2.323	0.2705				
VV Pyx	A	2.101	2.488	0.1578	0.0215	0.0661	0.0876	0.0039 ± 0.0012
	B	2.099	2.488	0.1572				
EK Cep	A	2.029	2.377	0.05895	0.0153	0.0575	0.0728	0.0030 ± 0.0009
	B	1.246	1.867	0.04084				
V1143 Cyg	A	1.391	2.351	0.02735	0.0106	0.0823	0.0929	0.00195 ± 0.00011
	B	1.347	2.288	0.02657				

^aRadii R in solar units.

^bMultiply tabular value by 10^{-4} .

EM Car V478 Cyg CW Cep QX Car CV Vel U Oph

zeta Phe IQ Per PV Cas AI Hya VV Pyx RS Cha

EK Cep MY Cyg PV Pup DM Vir V1143 Cyg UX Men